An asymmetric upwind flow, Yellow Sea Warm Current: 2. Arrested topographic waves in response to the northwesterly wind

Xiaopei Lin[1] and Jiayan Yang[2]

Received 10 July 2010; revised 23 February 2011; accepted 14 March 2011; published 29 April 2011.

[1] A warm and salty water mass exists along the Yellow Sea Trough (YST) in winter. This oceanic water mass is distinct from the ambient shelf water and is distributed on the western side of the YST. It has long been reasoned that a Yellow Sea Warm Current (YSWC) must exist. A recent observational study indeed supports the existence of the YSWC and shows that its position moved progressively westward as the warm water intrudes further shoreward toward the northwest. In this paper, we explain mechanisms for sustaining the YSWC and for its westward displacement. The northwesterly monsoonal wind prevails in the winter and is directed against the YSWC. The cross-trough scale is small compared with the spatial scale of monsoonal variation, so one can assume, to the first order, that the wind stress is uniform across the trough. The curl of depth-averaged wind stress has opposite signs on the two sides of the trough. Consequently, two oppositely rotating gyres develop initially and they converge along the trough giving rise to a barotropic upwind flow. But this upwind flow lasts only for a few days as the two gyres evolve and propagate as topographic waves. For a northerly wind, both gyres move westward since the positive (negative) potential vorticity flux on the western (eastern) side of the trough pushes the water toward shore (trough). If the bottom friction is negligible, the steady response becomes a large anticyclonic gyre over the trough and the upwind current is squeezed toward the shore line. In this case, no YSWC is sustained along or near the trough. This runaway warm current can be arrested by a moderate bottom friction. We therefore propose that the YSWC is actually arrested topographic waves in response to local wind stress forcing.

Citation: Lin, X., and J. Yang (2011), An asymmetric upwind flow, Yellow Sea Warm Current: 2. Arrested topographic waves in response to the northwesterly wind, *J. Geophys. Res.*, *116*, C04027, doi:10.1029/2010JC006514.

1. Introduction

[2] Continental shelves often serve as buffer zones, restricting the direct influence of deep oceanic processes on coastal seas. Consequently, the characteristics of the shelf water are distinctly different from those of the deep ocean off the continental slope. The ocean-sea contrast in water mass properties can be particularly pronounced in winter when intense air-sea flux affects the whole water column over shelves. For example, the winter water mass on the East China Sea shelf and in the Yellow Sea is significantly colder and fresher than that in the Kuroshio Current along the continental slope in the East China Sea. A noticeable exception is the presence of a warm and salty water mass along the Yellow Sea Trough (YST). This hydrographic feature was noted first by *Uda* [1934, 1936] who argued that a Yellow Sea Warm Current (YSWC) (Figure 1, red solid line) must exist. The distribution and variability of the warm water along the YST have been studied by many investigators since then. The warm water intrusion along the YST is a winter-only feature [*Lie*, 1986; *Park*, 1986; *Lie et al.*, 2000]. So the YSWC has been considered in some studies as a sporadic event in winter when the strong northwesterly monsoon prevails over the Yellow Sea [*Hsueh et al.*, 1986; *Hsueh*, 1988].

[3] The existence of the YSWC has been a subject of debate. *Lie et al.* [2001, 2009] questioned the existence of the YSWC by noting that the current was hypothesized mainly based on the T-S distribution rather than direct current measurements. They found that the along-trough velocity was very weak in all direct current measurements that were available to them and they concluded that the YSWC is an intermittent upwind flow when the western front of the Cheju Warm Current collapses during northerly wind bursts. A persistent seasonal current, they argued, does not necessarily exist.

[4] In a recent study, *Lin et al.* [2011] noted that most observations used in previous analyses, including those by *Lie et al.* [2009], were made in the central and on the eastern

[1]Physical Oceanography Laboratory, Ocean University of China, Qingdao, China.
[2]Department of Physical Oceanography, Woods Hole Oceanographic Institution, Woods Hole, Massachusetts, USA.

0148-0227/11/2010JC006514

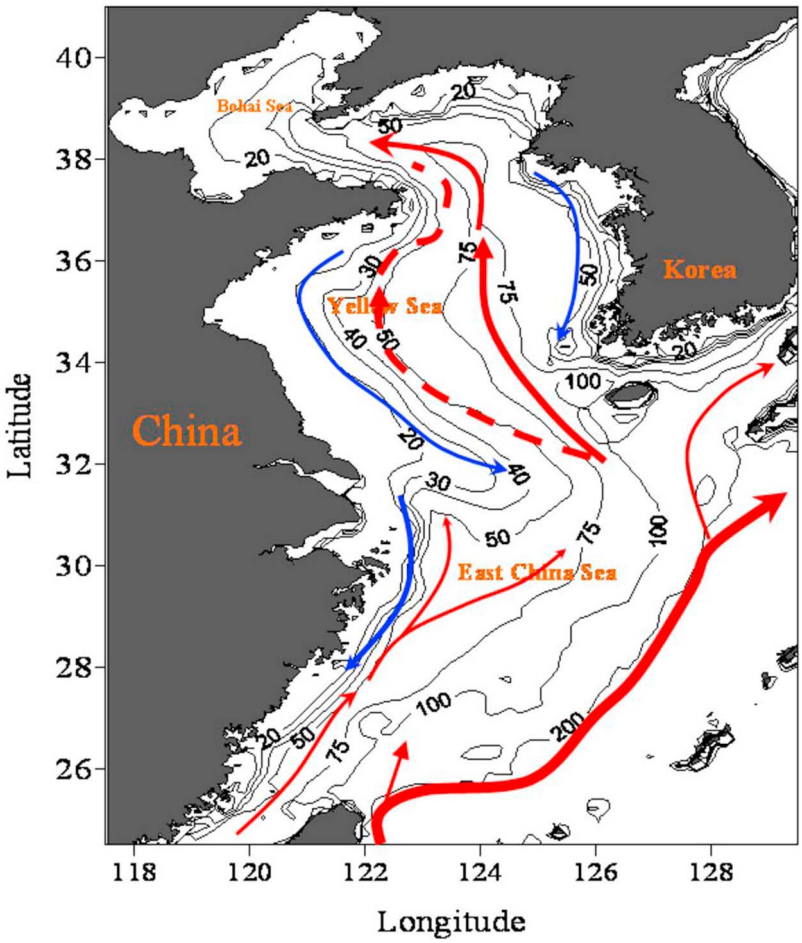

Figure 1. Schematic map of the winter circulation in the Yellow Sea and East China Sea. The red arrows denote the warm currents and the blue arrows denote the cold currents. The black lines are the bathymetry with 50, 100, and 200 m labeled. The dashed line in the Yellow Sea shows the pathway of the YSWC deduced from the recent observations.

(Korean) side of the YST. Data collected on the western (Chinese) side of the YST had not been accessible. The core of the warm water intrusion is actually along the western (Chinese) side of the YST [e.g., *Tang et al.*, 2001; *Huang et al.*, 2005] from where the data were missing in most previous studies. The existence of the YSWC would be hard to confirm without data from the western trough. *Lin et al.* [2011] analyzed in situ observations from Chinese sources, including a 31 year record of hydrographic surveys along 34°N, 35°N, and 36°N, and a large-scale observational program conducted simultaneously by three research vessels in the winter of 2006–2007. The latter included 6 moorings with ADCPs and more than 350 hydrographic stations. They also examined the sea surface temperature (SST) and surface wind from satellite sensors. Their study shows that a persistent winter YSWC indeed exists, but its axis is shifted upslope toward the western side of the trough (Figure 1, red dashed line in the Yellow Sea). This could explain why the current was weak along the central trough in the data analyzed by *Lie et al.* [2009]. With the confirmation of YSWC's existence, the following remain to be explained: how the YSWC is formed and maintained as a seasonal mean current (in contrast to a sporadic current in response to synoptic forcing) and why the current is on the western side of the trough. This study attempts to address these questions.

[5] There have been only a handful of studies addressing why the YSWC moves gradually upslope toward the west. *Xie et al.* [2002] suggested that the westward Ekman transport induced by a northerly wind could be responsible for the shift. In situ observations, however, show that the whole warm water column, not merely the Ekman layer, is shifted westward [*Lin et al.*, 2011]. *Huang et al.* [2005] attributed the westward shift of the YSWC to the surface cooling and self-advection of baroclinic currents. But both numerical simulations and observations show that it is the barotropic current that is primarily responsible for the westward shift of the warm tongue [*Lie et al.*, 2009; *Moon et al.*, 2009; *Lin et al.*, 2011]. The dynamics of the asymmetric upwind YSWC remain to be further explored.

[6] In this paper, we will try to explain why the YSWC is shifted to the western side of the YST. In section 2 we will discuss the leading dynamical balance in a simple barotropic model and show the key dynamical processes of wind forcing on a varied bathymetry. Results from some additional numerical experiments will be presented, in section 3,

to elucidate the role of friction. Further discussion and a brief summary will be given in sections 4 and 5 respectively.

2. The Dynamics of an Upwind Current in a Barotropic Model

[7] The YSWC strengthens in response to bursts of the northerly wind [*Hsueh and Pang*, 1989]. Similar responses have been observed in along-trough flows in large lakes or in narrow estuaries [e.g., *Rao and Murthy*, 1970; *Csanady*, 1973, 1982]. *Csanady* [1982] discussed in detail the interplay of wind stress, pressure gradient and friction that give rise to an upwind current response along a trough. In the shallowest regions along the boundary in a lake or estuary, the wind stress is the dominant forcing and thus the rim currents are in the same direction as wind. The boundary currents on both sides of the trough flow in the same direction and pile up water mass at the downwind end of the lake or estuary. Along the trough the water is deep. The depth-averaged wind stress is small and too weak to counter the pressure gradient in the along-trough direction. This imbalance results in a pressure-driven flow that is opposite to the direction of the surface wind. Together with two rim currents this forms double gyres in a closed basin [*Csanady*, 1982]. This classic pattern of an upwind flow along the trough, sandwiched by two downwind boundary currents, indeed bears some similarity to the YSWC schematized in Figure 1 (red solid line in the Yellow Sea). Thus, the upwind flow theory has been used to interpret the formation of the YSWC [*Hsueh and Pang*, 1989; *Hsueh and Yuan*, 1997; *Isobe*, 2008]. Other studies such as *Mask et al.* [1998], *Riedlinger and Jacobs* [2000], and *Teague and Jacobs* [2000] also showed that the YSWC response to northerly wind bursts. In a nonrotational model, the upwind current is typically strongest along the trough. This is quite different from the YSWC where the core of the current is not exactly along the trough axis but shifted noticeably westward.

[8] The rotational effect can be ignored if the lake or estuary is sufficiently small compared with the barotropic deformation radius (which is about 300 km for a basin with water depth of 100 m in a typical midlatitude location where the Coriolis parameter $f \sim 10^{-4}$ s^{-1}). However, when the rotational effect becomes important, such as for the scale of the YSWC, the flow pattern becomes considerably different. The response is influenced by the propagation of topographic Rossby waves [*Csanady*, 1982; see also *Takahashi et al.*, 1995; *Winant*, 2004].

[9] Here we start with a simple linear, one-layer ocean model to explain the westward shift of the YSWC. The barotropic model is adequate for modeling the leading order dynamics and has been applied in many process-oriented studies previously (see *Brink* [1998] for a review). Some justifications of using this simple model will be given in section 4. The model is governed by the following equations:

$$\begin{aligned} \frac{\partial u}{\partial t} - fv &= -g\frac{\partial \eta}{\partial x} + \frac{\tau_s^x - \tau_b^x}{\rho H} \\ \frac{\partial v}{\partial t} + fu &= -g\frac{\partial \eta}{\partial y} + \frac{\tau_s^y - \tau_b^y}{\rho H}, \\ \frac{\partial \eta}{\partial t} + \frac{\partial (Hu)}{\partial x} + \frac{\partial (Hv)}{\partial y} &= 0 \end{aligned} \tag{1}$$

where η is the sea surface height (SSH), $H(x,y)$ the mean water depth, u and v the lateral velocity components, τ_s and τ_b the surface and bottom stresses, and ρ the water density. This model was used by *Yang* [2007] to investigate the upwind Taiwan Warm Current in the East China Sea. The model domain used in this study is a closed basin of 8° × 45° in the zonal and meridional directions, respectively, as shown in Figure 2. South of 45°N, there is a meridional trough with water depth reaching 100 m in the center of the basin. The depth decreases gradually in the y direction north of 45°N. This bathymetry is an idealized domain meant to represent the YST shown in Figure 1. For a relatively small domain with large bathymetric variations, like the one used here, the potential vorticity (PV) gradient is dominated by variations in H rather than f. So the model (1) is formulated on an f plane with the Coriolis parameter set to its value at 35°N. We use a spatial resolution of 1/16° both zonally and meridionally. The model is forced by a constant northerly (southward) wind stress of 0.1 N m^2, i.e., $(\tau_s^x, \tau_s^y) = (0, -\tau_0)$, which is a typical magnitude for winter wind stress in the Yellow Sea. A linear drag is used for the bottom friction, i.e., $\vec{\tau}_b = \lambda \vec{u}$, consistent with many previous studies [*Hsueh and Pang*, 1989; *Pringle*, 2002]. A drag coefficient, $\lambda = 5 \times 10^{-4}$ [*Chapman*, 1987], is used for the linear bottom friction in the northern half model domain. To avoid the effect of southern boundary, we conducted the model experiments with a very long model domain of 45° meridionaly and placed a sponge layer in the southern half model domain (the drag coefficient λ increasing gradually to 5×10^{-2}). This formulation dampens the outward propagating signals and effectively prevents them from reentering the northern domain.

[10] We only plot the flows in the northern part of the model domain for a better illustration purpose. The steady velocity field from the first model experiment (EXP1) is shown in Figure 3a. Two gyres emerge in response to the wind stress forcing. The circulation is cyclonic on the western side of the trough and anticyclonic on the eastern side. Associated with these two oppositely rotating gyres are two coastal currents along the basin's eastern and western boundaries. They both flow in the same direction as the surface wind. Along the trough, the confluence of the two gyres gives rise to a northward upwind current. The spatial structure of the circulation, i.e., an upwind current along the trough, sandwiched by two downwind coastal currents, is similar, in a broad sense, to the observed Yellow Sea current system shown schematically in Figure 1. South of 45°N, the upwind current does not flow along the axis of the trough, but is shifted northwestward. This westward shift is clearly shown in a meridional velocity section along 44°N in Figure 3b. The axis of the northward upwind current is shifted about 1° west of the central trough axis.

[11] Large-scale flows over varying bathymetry can often be elucidated best in terms of vorticity and PV dynamics. A large-scale ocean current tends to flow along PV contours. Flows that cross PV contours are most often driven by atmospheric forcing, friction, and eddy PV flux. In shallow water with a large variation of topography, like the YS, the PV distribution is largely set by the bathymetry. So the westward shift of the upwind current represents a considerable PV advection and thus needs to be

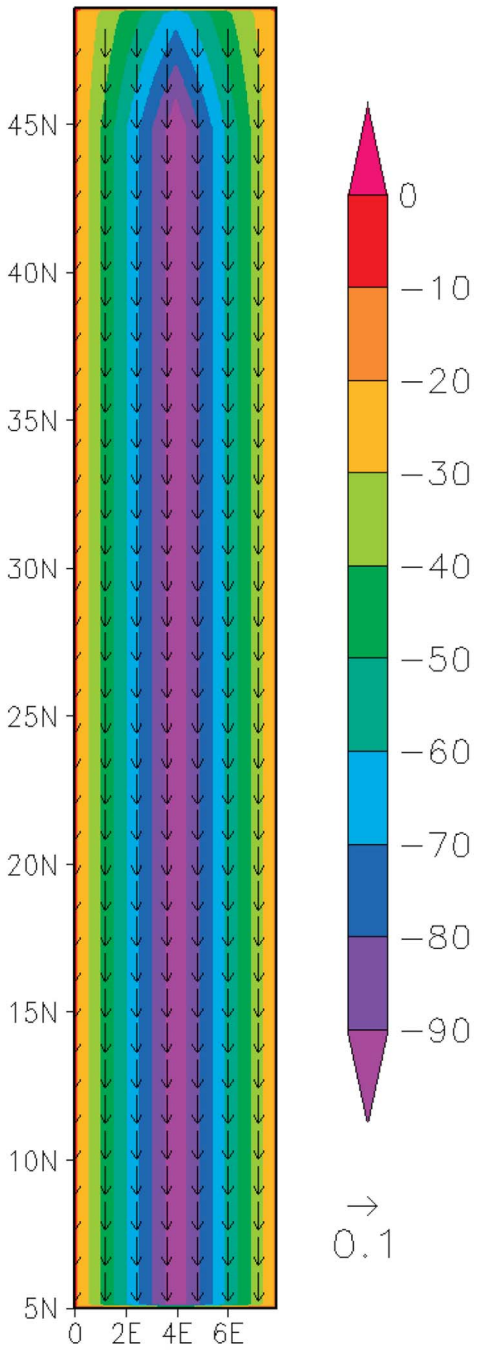

Figure 2. The model domain in the 2-D model experiments. Color shading represents the bathymetry (m). Black arrows are the wind stress (N m^2) used in EXP1.

balanced by a forcing term. The vorticity equation from equation (1) is

$$\frac{\partial \zeta}{\partial t} = \frac{f}{H}(\vec{u}\cdot\nabla H) - \frac{1}{\rho}\frac{\partial}{\partial x}\left(\frac{\tau_0}{H}\right) + \frac{f}{H}\frac{\partial \eta}{\partial t} + F_b, \tag{2}$$

where $F_b = -\frac{\lambda}{\rho}\left[\frac{\partial}{\partial x}\left(\frac{v}{H}\right) - \frac{\partial}{\partial y}\left(\frac{u}{H}\right)\right]$ is the curl of the bottom stress. The change is caused by PV advection across isobaths, wind stress curl, vortex stretching and dissipation by bottom friction. If we further assume, without losing generality, that H varies only in the x direction, such as in the trough region, the PV equation becomes

$$\frac{\partial \zeta}{\partial t} = \frac{f}{H}(\vec{u}\cdot\nabla H) - \frac{1}{\rho}\frac{d}{dx}\left(\frac{\tau_0}{H}\right) + \frac{f}{H}\frac{\partial \eta}{\partial t} + F_b. \tag{3}$$

In the steady state, equation (3) becomes

$$\beta_T u = -\frac{1}{\rho}\frac{\partial}{\partial x}\left(\frac{\tau_0}{H}\right) + F_b, \tag{4}$$

where $\beta_T = -\frac{f}{H}H_x$ is the cross-isobathic vorticity gradients (or the more commonly called topographic beta). Equation (4) is the zeroth-order vorticity balance in a barotropic model forced by a uniform meridional wind stress. In this model, a uniform wind stress over a varying bathymetry results in a differential distribution of the depth-averaged stress. The curl of this stress is balanced both by the frictional vorticity sink, F_b, and by the vorticity advection, $\beta_T u$. The latter represents a cross-isobathic vorticity advection. Here we consider the idealized "V" shape topography of the YST as shown in the model bathymetry in Figure 2. For a uniform northerly wind stress, the curl of the depth-averaged stress is positive on the western side of the trough and negative on the eastern side. If the torque of the bottom friction, F_b, does not balance the depth-averaged wind stress, a northwestward velocity over the western half of the domain and a southwestern velocity on the eastern half must result (on the western side, the positive stress curl pushes the water shoreward toward a higher f/H, while on the eastern side the negative curl forces flow toward the trough where f/H is smaller).

[12] The model PV balance is diagnosed here (Figure 4). Planetary PV, f/H, and its variations, not shown, are determined solely by H in this f plane model. The curl of a uniform northerly wind stress, τ_0, is zero. But the curl of the depth-averaged stress, τ_0/H, is nontrivial due to the variation of water depth. Because the bathymetry is zonally symmetric along the trough, the curl of the depth-averaged wind stress is antisymmetric about the trough (Figure 4a). The dissipation, i.e., the curl of depth-averaged bottom friction, is large along the boundaries where the flow is strong and water is shallow (compare Figures 4b and 4a). It is also considerable on the western trough where the upwind current is strong. The curl of τ_0/H is negative on the eastern trough, and this negative PV flux input by wind would push the water toward a lower PV region according to equation (4), namely, toward the trough where H is large. On the western trough, on the other hand, the curl is positive and thus the flow is forced toward shallower region, i.e., upslope and away from the trough. As a consequence to this wind stress forcing, there is a net transport of water mass across the trough from the eastern to the western basin in the interior. This balance of PV advection with the PV residual term between the wind and friction can be clearly seen in Figures 4c and 4d. The return flow to the east then occurs along the northern boundary as shown in Figure 3. This is the main reason why the northward upwind current is shifted to the western side of the trough.

3. The Role of Friction

[13] The above analysis indicates that the interplay between the depth-averaged wind stress and friction determines the

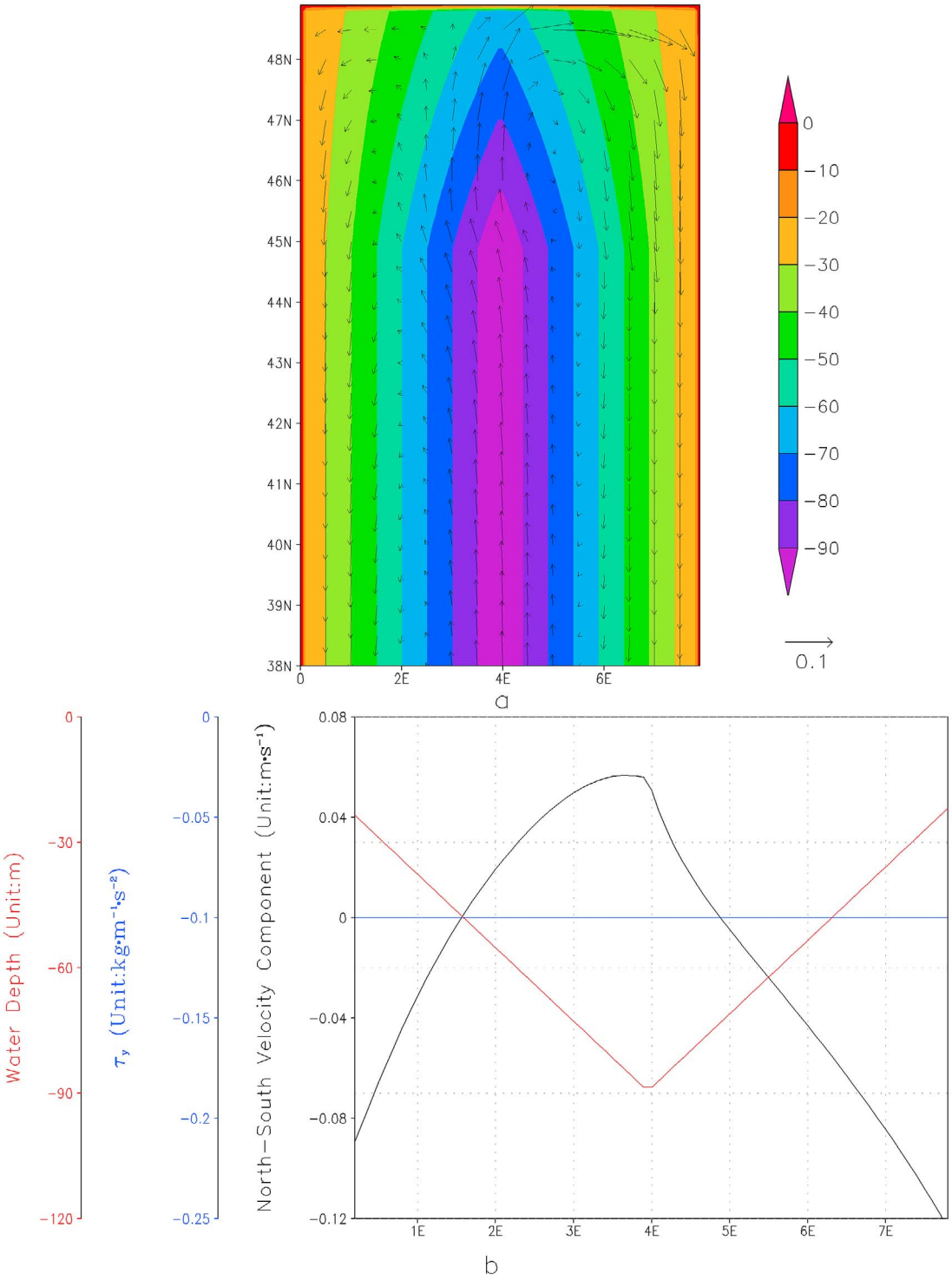

Figure 3. (a) The current field (m s^{-1}) in EXP1, with the bathymetry (m) in color shading. (b) The meridional current speed (black line, m s^{-1}), wind stress (blue line, $kgm^{-1}s^{-1}$), and water depth (red line, m) along a section at 44°N in EXP1.

structure of the upwind current. In this section, to further examine the role of friction in setting the position of an upwind current, we discuss two extreme cases, one with a very small friction and the other with a very large friction. We ran the model with a much smaller ($\lambda = 5 \times 10^{-5}$, EXP2) and a larger ($\lambda = 5 \times 10^{-3}$, EXP3) bottom drag coefficient in the northern half model domain. All other parameters remain the same as those used in EXP1.

[14] Before we show the model results from the experiment with a small drag coefficient, we discuss the vorticity

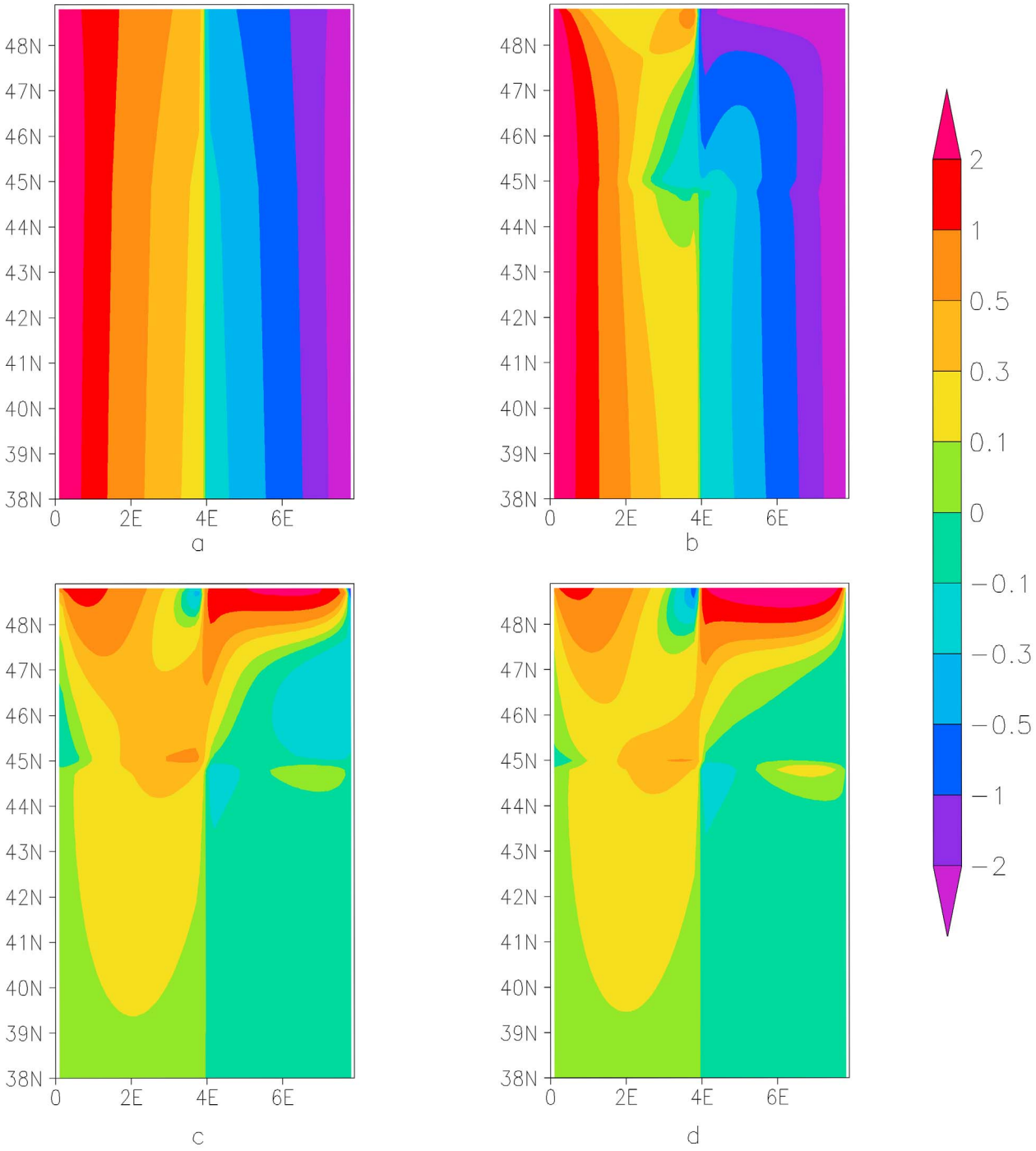

Figure 4. The PV budget in EXP1 (10^{-7} m^{-1} s^{-1}). (a) PV input by the wind stress. (b) PV input by bottom friction. (c) PV residual term between the wind and bottom friction. (d) PV advection due to the topography vorticity gradient.

balance in the limit of no drag. If the bottom friction is negligible, i.e., $F_b = 0$, equation (4) is reduced to the classic Ekman transport equation

$$u = -\frac{\tau_0}{\rho f H}. \tag{5}$$

In this limit, uniform southward wind drives a persistent westward current. The westward flow results in a convergence (divergence) along the western (eastern) boundary. Boundary currents then close the circulation. In this case, a large anticyclonic gyre is established. This essentially explains the dynamics underlying the model results produced by

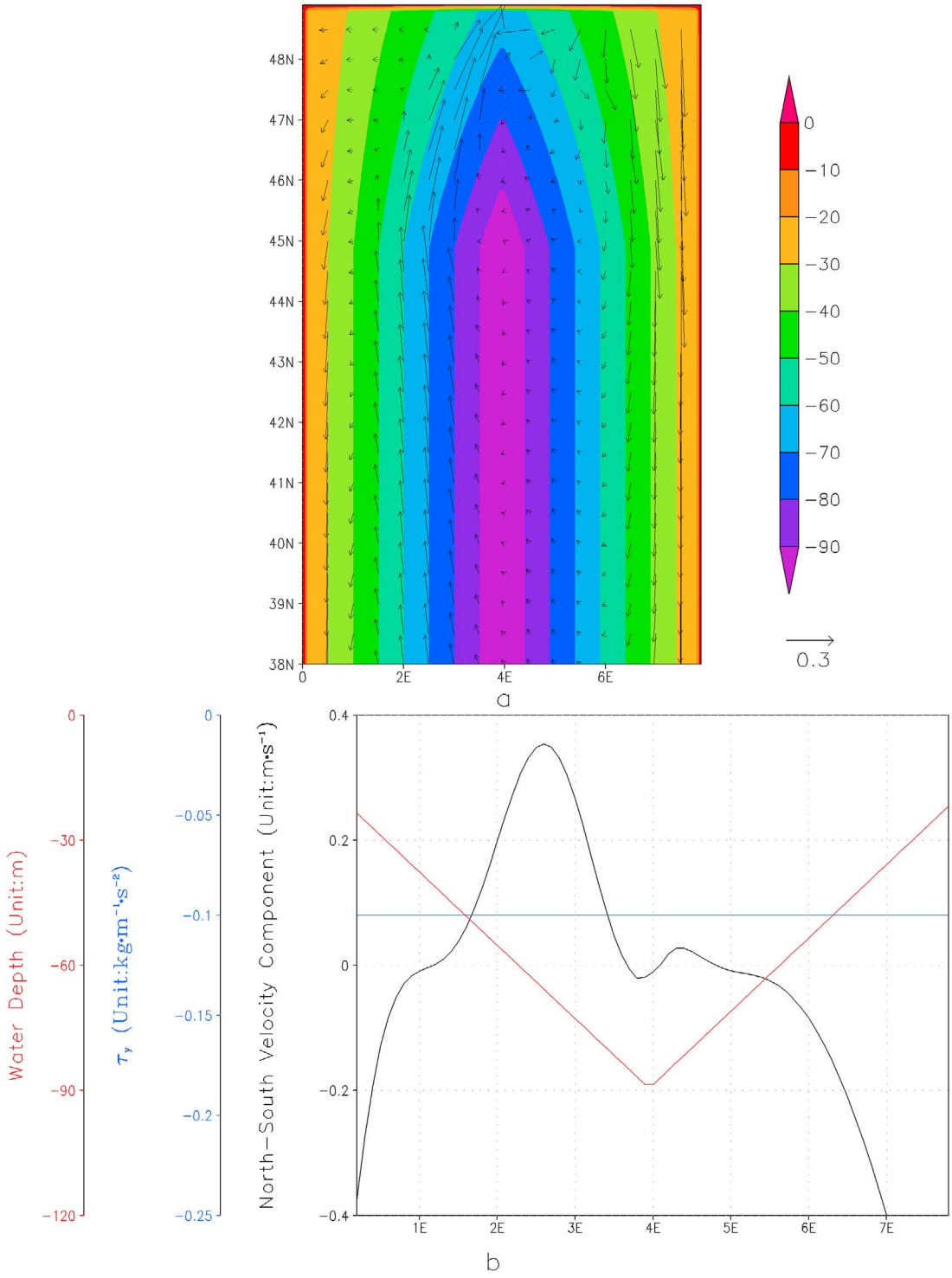

Figure 5. The same as Figure 3 but for EXP2 (small bottom friction).

Takahashi et al. [1995]. In their model, the upwind current was located near the western boundary instead of along the trough. This is demonstrated in our experiment with small drag coefficient, EXP2 (Figure 5a). Compared with EXP1, the anticyclonic gyre in EXP2 extends further across the trough into the western side of the trough. The upwind current is stronger than that in EXP1 and is located closer to the western boundary. In the trough region, the current is basically directed westward as predicted by equation (5) and eventually joins the northward upwind current on the western

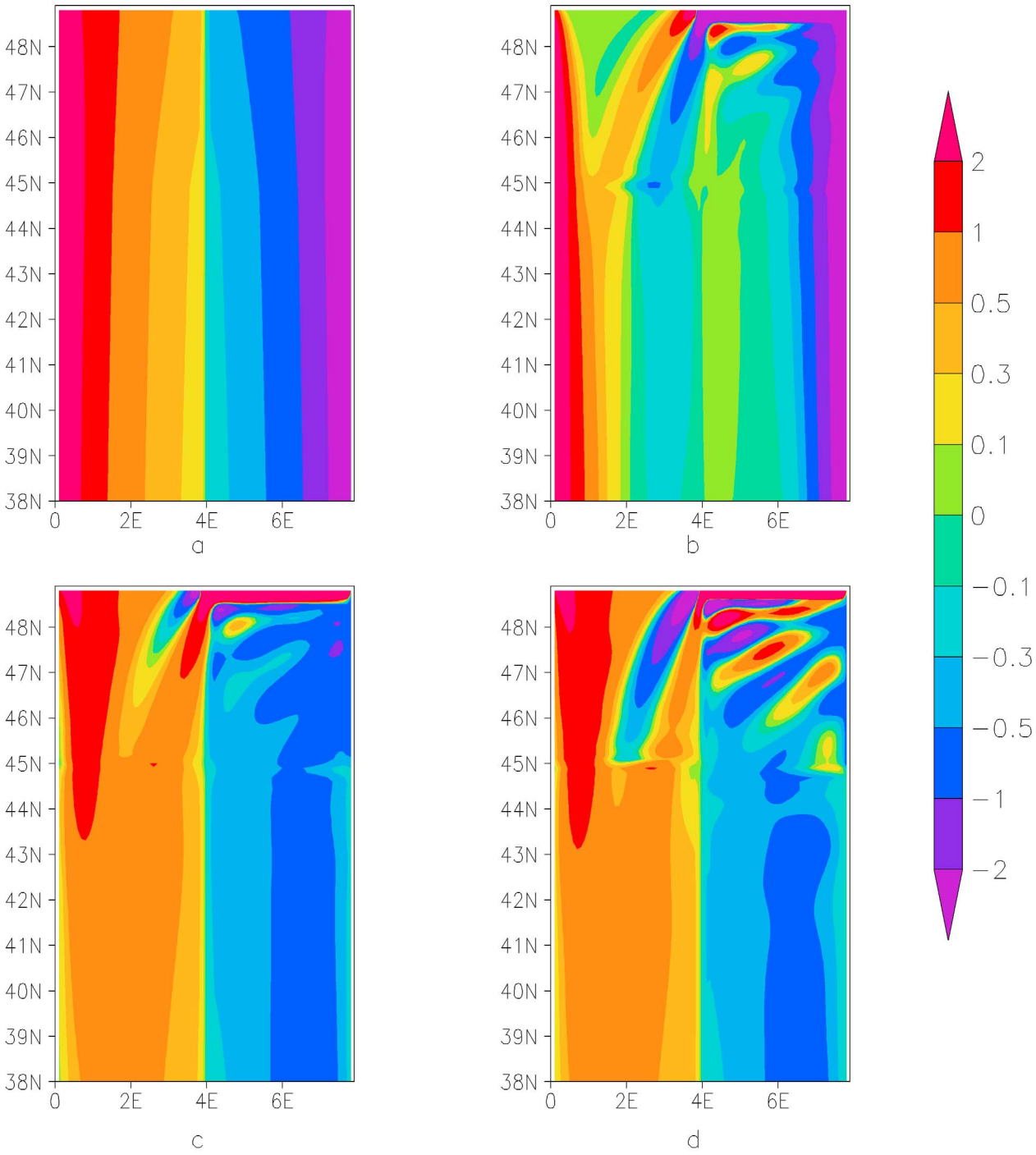

Figure 6. The same as Figure 4 but for EXP2 (small bottom friction).

side of the trough. The large shift of the upwind current can also be seen from Figure 5b. The axis of the upwind current at 44°N is about 2° west of the central trough. The westward and cross-trough advection is important in the PV balance as shown in Figure 6. The balance is mainly between the curl of depth-averaged wind stress and the westward advection in the trough region.

[15] The analyses above suggest that in a simple model as that described by equation (1), an upwind current cannot be sustained in the trough region without the bottom friction. Now let us examine further the role of bottom friction on the steady state solution. For a simple linear friction, i.e., $\vec{\tau}_b = \lambda\vec{u}$, the dissipation term is

$$F_b = -\frac{\lambda}{\rho}\left[\frac{\partial}{\partial x}\left(\frac{v}{H}\right) - \frac{\partial}{\partial y}\left(\frac{u}{H}\right)\right]. \quad (6)$$

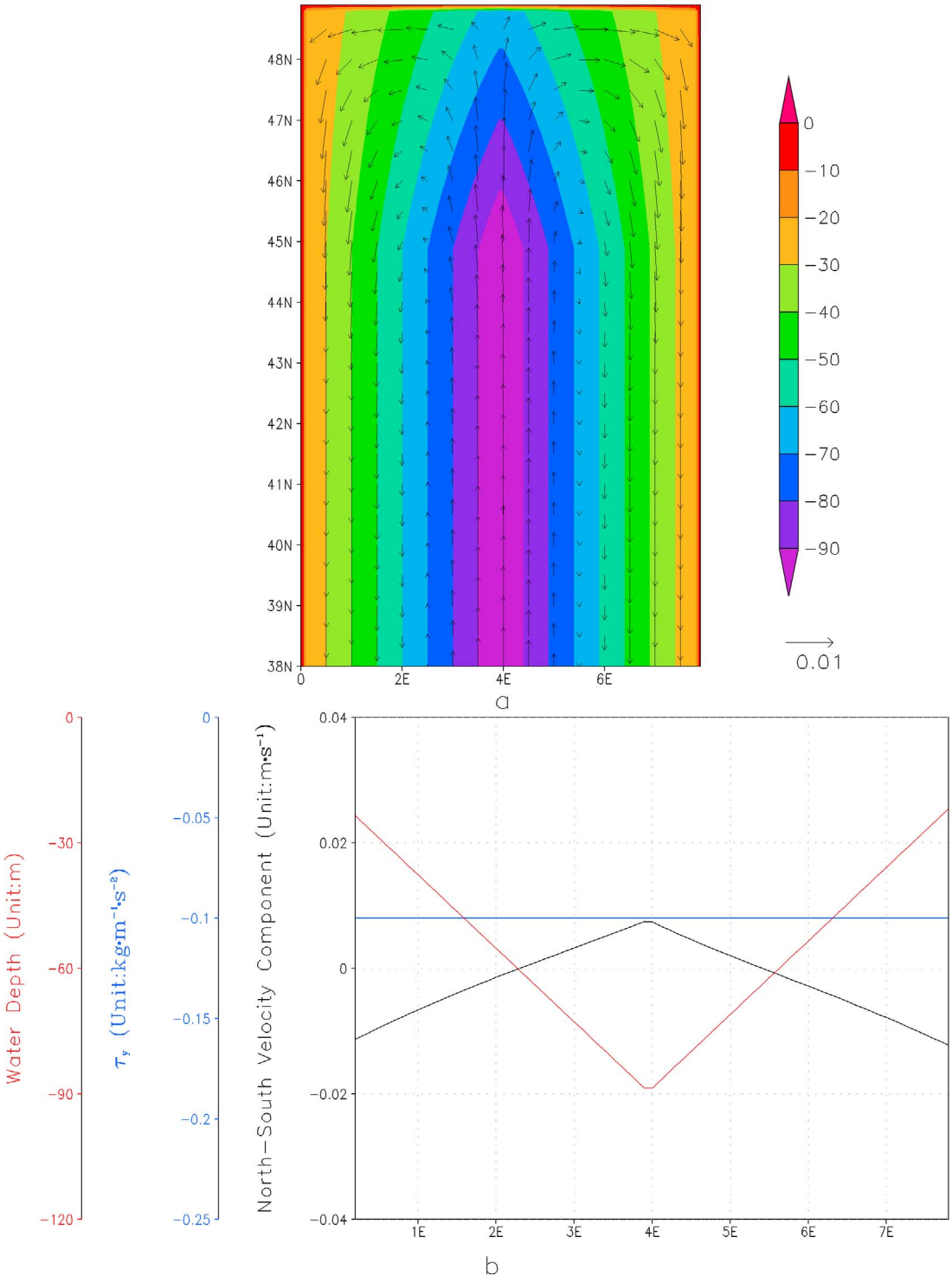

Figure 7. The same as Figure 3 but for EXP3 (large bottom friction).

Since the upwind current has a smaller scale in the zonal direction than that in the meridional direction, the bottom friction can be approximated by the first term on the RHS of equation (6). The steady version of equation (3) is

$$\beta_T u \approx -\frac{1}{\rho}\frac{d}{dx}\left(\frac{\tau_0}{H}\right) - \frac{\lambda}{\rho}\frac{\partial}{\partial x}\left(\frac{v}{H}\right). \tag{7}$$

For the limit of a very large friction coefficient, the wind stress induced PV flux will basically be balanced by the dissipation. Equation (7) can be further approximated by

$$\frac{\partial}{\partial x}\left(\frac{\lambda v}{H}\right) \approx -\frac{d}{dx}\left(\frac{\tau_0}{H}\right). \tag{8}$$

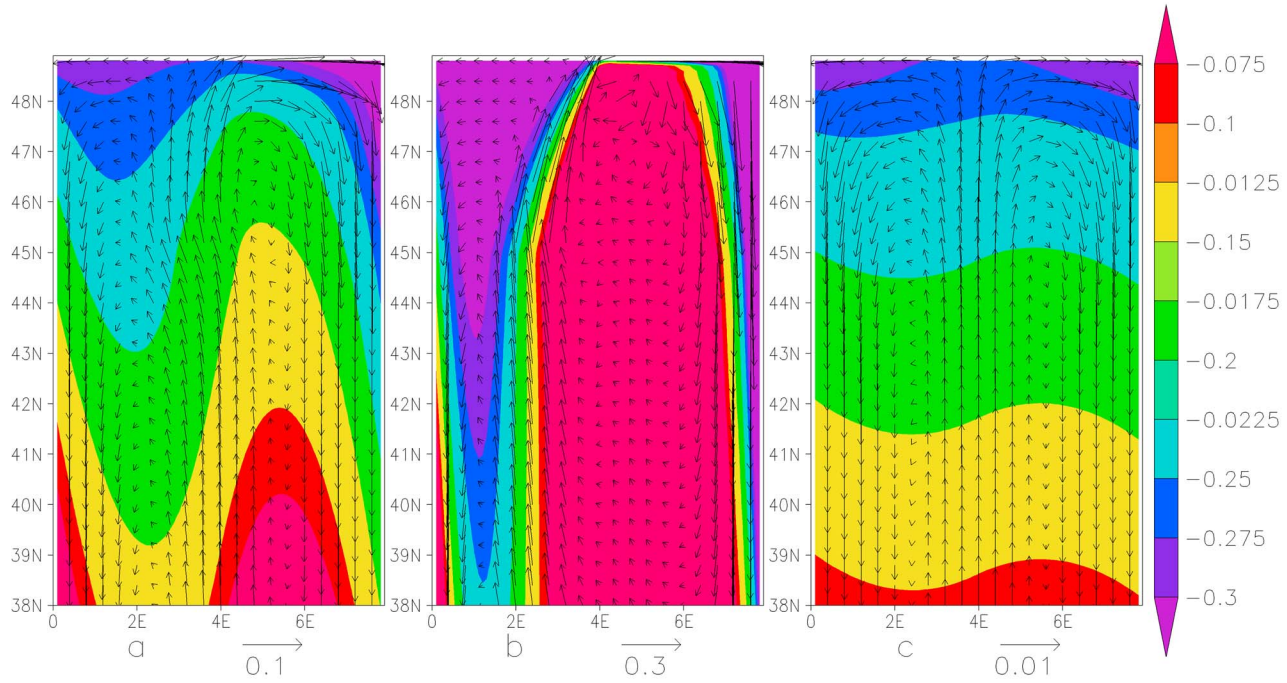

Figure 8. The steady state for the three experiments: (a) EXP1, (b) EXP2, and (c) EXP3. Color shading represents the sea surface height (m) and the black arrows are the current field (m s^{-1}).

The solution of equation (8) becomes

$$v(x,y) = \frac{C(y)}{\lambda} H(x) + \frac{\tau_0}{\lambda}. \tag{9}$$

Here $C(y)$ is determined by the boundary conditions. The solution (9) indicates that under a very strong bottom friction, the meridional current will have a zonal pattern similar to that of the bathymetry. Considering our "V" shape bathymetry as shown in Figure 2, there will be a symmetric upwind current along the central trough with a double gyre system (cyclonic in the west and anticyclonic in the east). The flow field in EXP3 (Figure 7), run with strong bottom friction, confirms this assessment. There is no westward shift and the two gyres are essentially symmetric about the trough.

[16] The steady state results from the three experiments demonstrate that the upwind current is driven by the wind stress and its position is strongly influenced by the friction. We next examine how bottom friction affects the spin-up of the circulation. Oceanic adjustment to the wind forcing is mainly through topographic waves and Kelvin waves. The initial response to the onset of the wind stress is governed by

$$\frac{\partial \zeta}{\partial t} = -\frac{\tau_0}{\rho} \frac{d}{dx}\left(\frac{1}{H}\right). \tag{10}$$

The right-hand side of equation (10) is positive and negative on the eastern and western sides of the trough, respectively. The initial oceanic response after a couple of days consists of two oppositely rotating gyres which converge along the trough, giving rise to a northward flow. This also explains the upwind response to northerly wind bursts by *Hsueh and Pang*'s [1989] model. But these initial fields tend to propagate as topographic waves along *f*/*H* contours, as explained by *Csanady* [1982]. The friction, however, determines the dissipation length scale. With the propagation of topographic waves, the upwind current also changes its position. For the small friction case (EXP2), the topographic waves can reach the western trough along the bathymetry and the northern boundary before being dampened. Figures 8a–8c shows the final steady states for the three experiments. It takes a longer time for EXP2 to reach its final steady state in which a high sea level occupies the central and eastern domain and a low sea level is located along the western boundary (Figure 8b). The double gyres become asymmetric and the upwind current is pushed to a position near the western boundary with a downwind current along the western boundary as described by *Takahashi et al.* [1995]. This also seems to explain the previous observations of currents in the central YST [*Hsueh*, 1988; *Lie et al.*, 2001, 2009] in which the upwind current occurred after strong northerly wind bursts and then disappeared in the central trough. When we use a very large friction (EXP3), the topographic waves are strongly dampened by the bottom friction and are arrested just near the central trough; the upwind current also occurs in the central trough as shown in Figure 8c. For the moderate friction case (EXP1), the bottom friction arrests the topographic waves on the western bank of the trough to maintain the PV balance there (Figure 8a). In such a case,

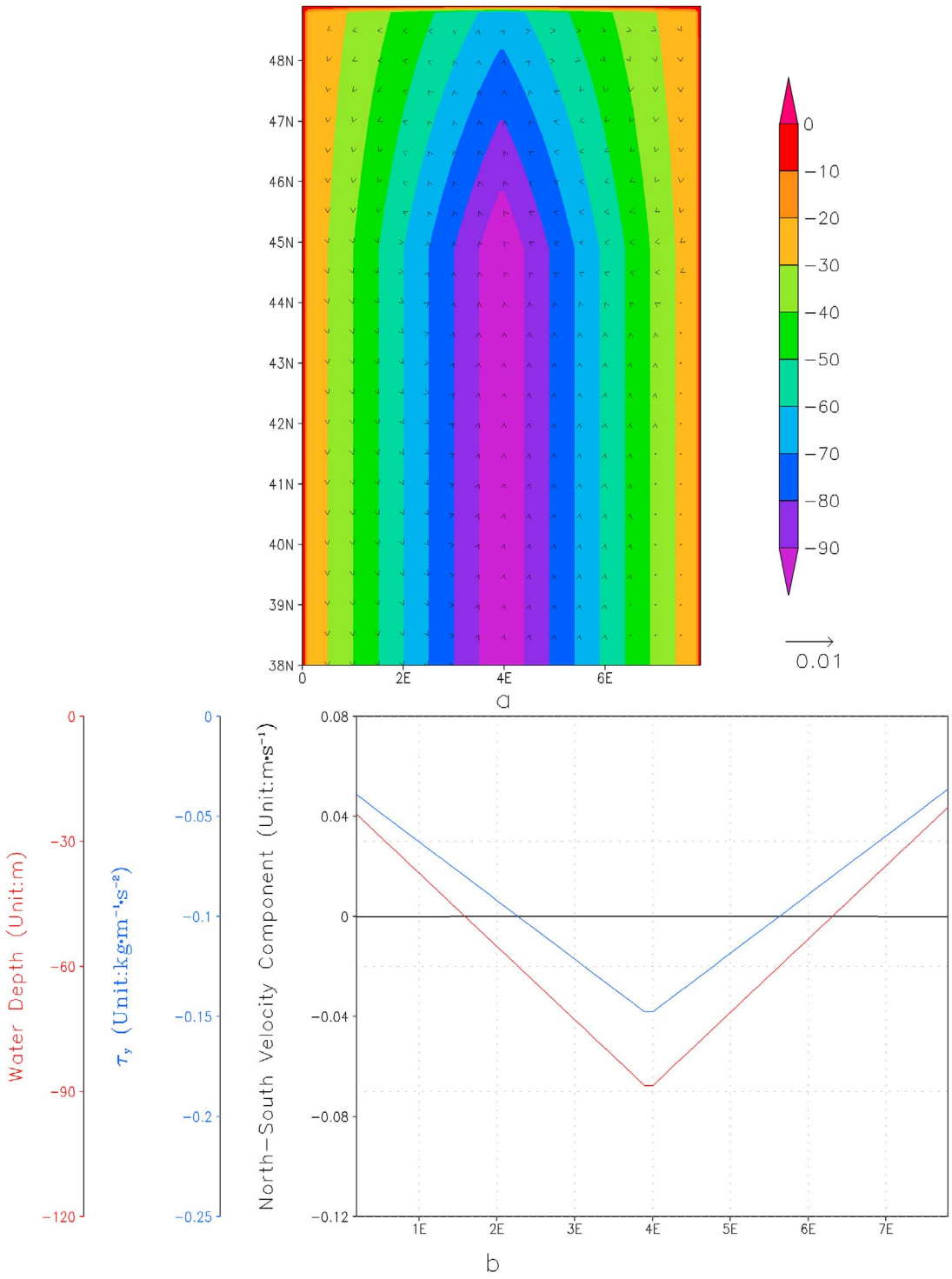

Figure 9. The same as Figure 3 but for EXP4 (τ_s/H = 0.0013).

the upwind current is located on the western trough. Thus, the dynamics underlying the observed westward shift and asymmetry of the YSWC are interpreted here as the frictionally arrested topographic waves, a type of shallow water waves discussed by *Csanady* [1978] and *Hetland et al.* [2001]. The propagating scale of arrested topography waves is proportional to $\frac{H_s f}{\lambda}$. This could essentially explain the difference of sea level anomaly pattern and position of upwind current axis in EXP2 and EXP3.

4. Discussions

[17] The results from three experiments show that (1) the upwind current and two coastal downwind currents are

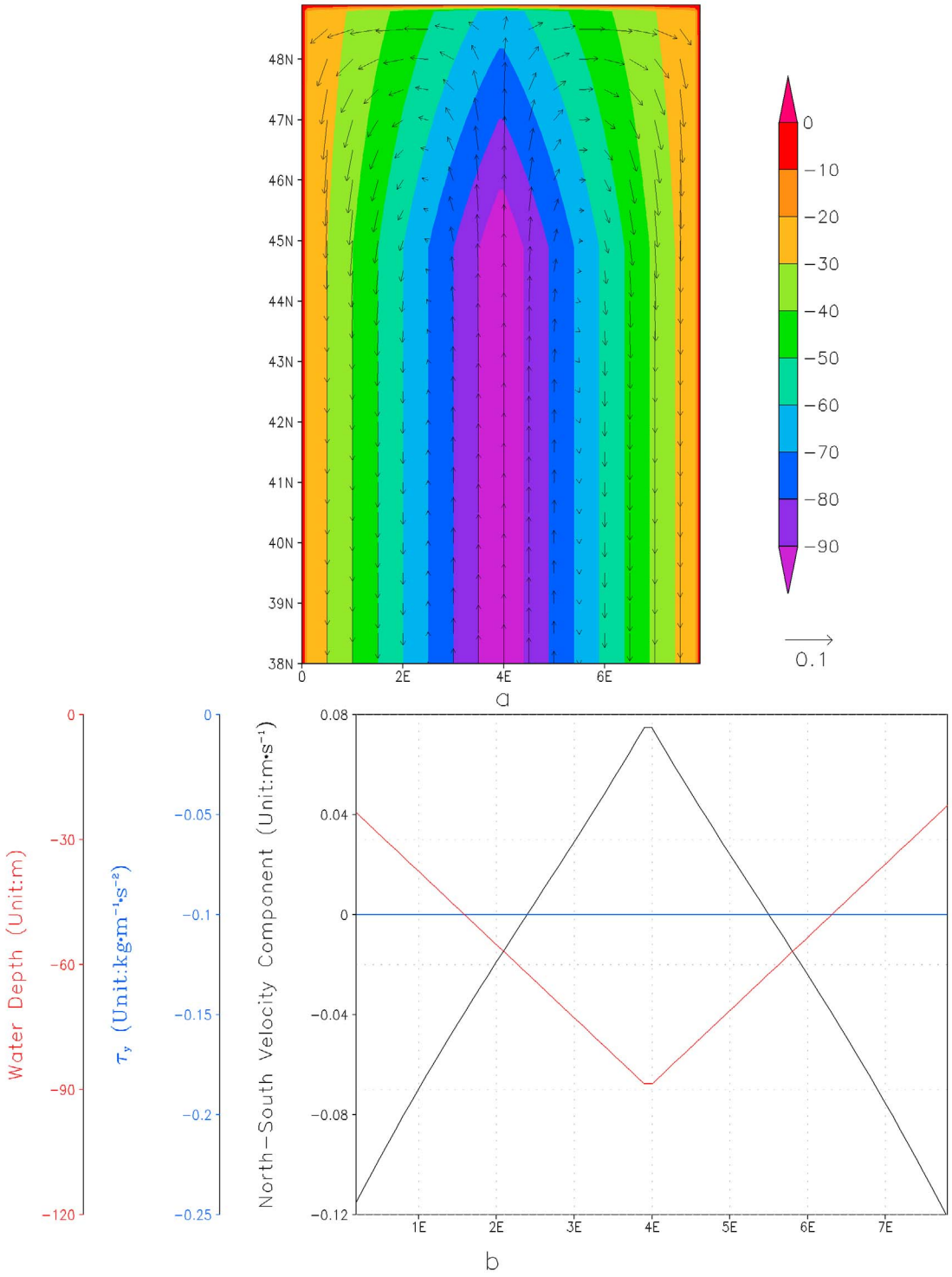

Figure 10. The same as Figure 3 but for EXP5 ($f = 0$).

associated with two oppositely rotating wind-driven gyres, (2) the two gyres are forced by the curl of depth-averaged wind stress and propagate as topographic waves along f/H contours and land-sea boundaries, (3) these waves can be arrested by friction, (4) the tendency of wave propagation causes the asymmetry of two gyres, and (5) this asymmetry results in the westward shift of the upwind current toward the western slope of the trough.

[18] In each of these results, the controlling parameter is the curl of τ_s/H rather than the curl of τ_s. One could change either τ or H, and the resulting barotropic flow will be similar, as long as the curl of τ_s/H remains unchanged.

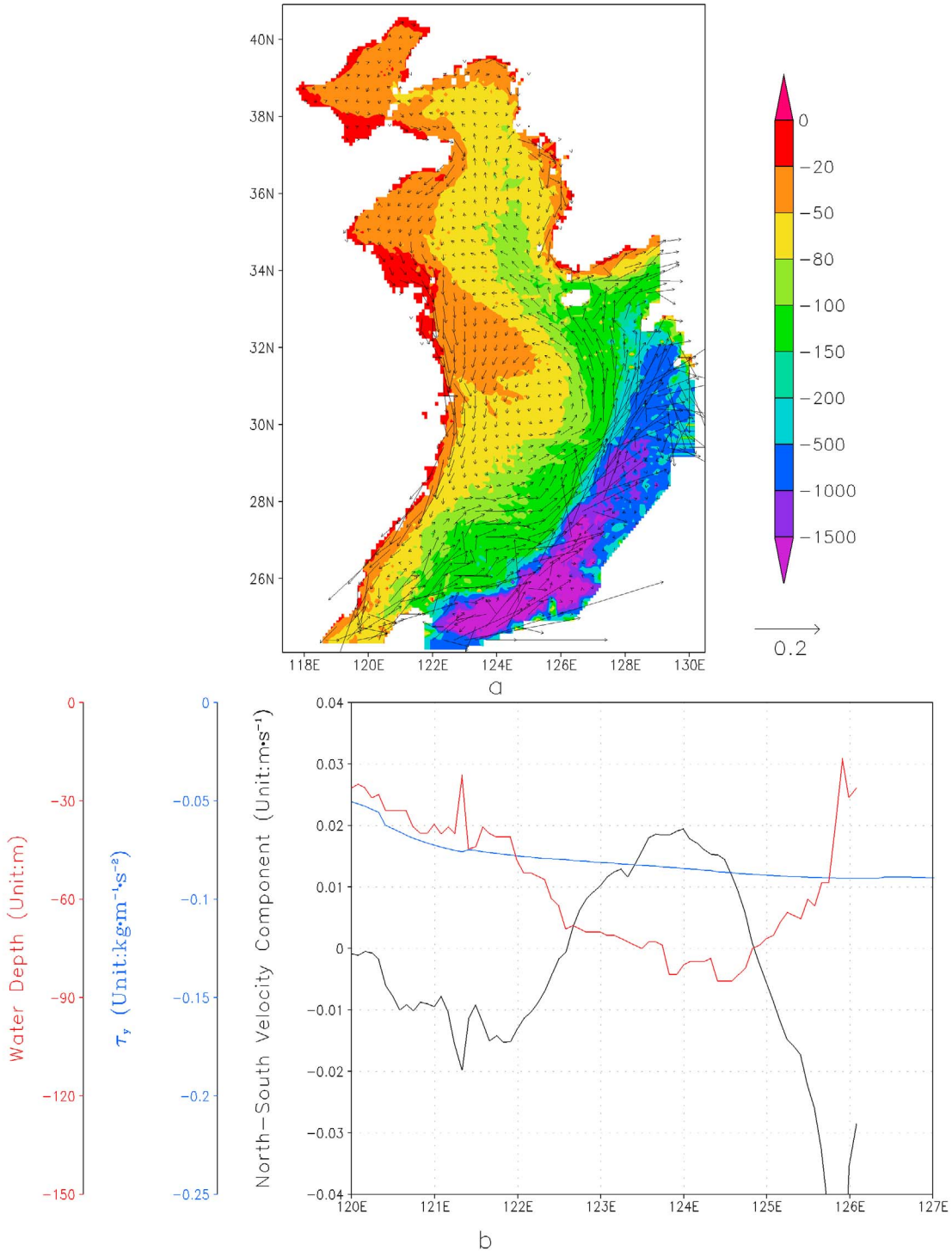

Figure 11. (a) The current field (m s^{-1}) from EXP6, with the bathymetry (m) in color shading. (b) The meridional current speed (black line, m s^{-1}), wind stress (blue line, kg m^{-1} s^{-1}), and water depth (red line, m) along a section at 35°N. In this experiment with realistic bathymetry and forcing, a moderate friction coefficient (5×10^{-4} s^{-1} m^{-1}) is used. The position of the YSWC, including the westward shift, is reasonably well simulated.

On the other hand, the flow will be different with different topography even if the model were forced by the same wind. Here we demonstrate these points with another experiment, EXP4, in which τ_s is kept proportional to H so that the curl of τ_s/H is zero (EXP4). Specifically, we set $\frac{\tau_0}{H} = 0.0013$ with H the same as in the previous experiments. This is equivalent to a wind stress of 0.1 N m^2 forcing a basin with water depth of 75 m. As expected, the model has a very weak

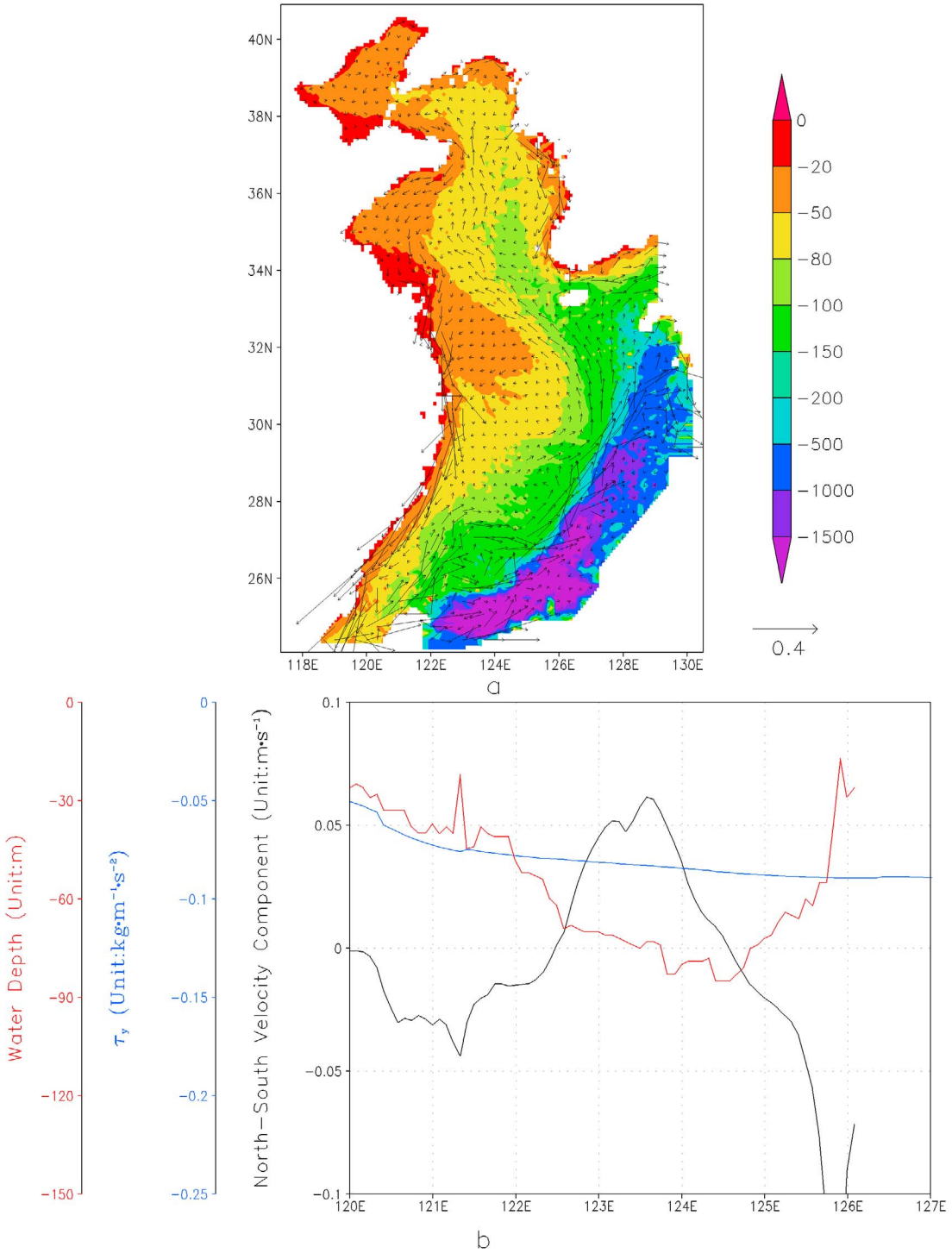

Figure 12. Result from EXP7 in which a small friction coefficient (5×10^{-5} s^{-1} m^{-1}) is used. Note that the axis of the northward current is shifted further westward as compared the results from EXP6 (shown in Figure 11).

response to the wind forcing (Figure 9a). There is only a weak flow in the basin and no obvious upwind or downwind flow in the meridional velocity section along 35°N (Figure 9b).

[19] Another important dynamic process in the formation of a westward shifted and asymmetric upwind current is related to the topographic vorticity advection, $\beta_T u$. This cross-isobathic velocity is responsible for the asymmetry of the upwind current. Topographic β, i.e., $\beta_T = -\frac{f}{H}\frac{\partial H}{\partial x}$, is not only determined by the bathymetry but also the Coriolis parameter f. How does the flow differ if the rotational effect is removed? In the next experiment (EXP5), we run the

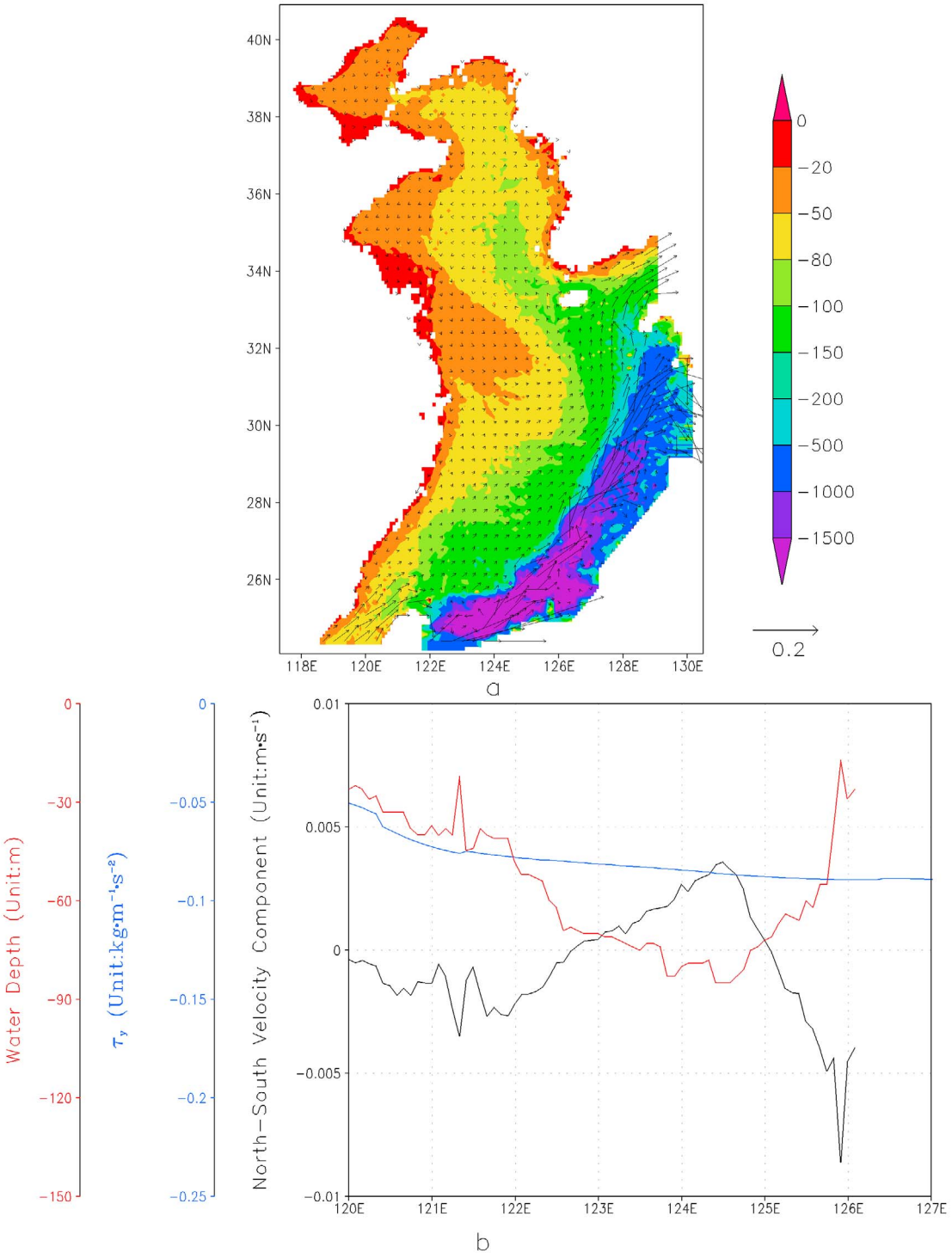

Figure 13. EXP8 with a large bottom friction. The current over the shelves is weak and the YSWC is now along the center of the YST.

model with $f = 0$. This experiment is similar to the discussion of upwind current in a bowl shape lake by *Csanady* [1982]. The flow, as shown in Figure 10, becomes symmetric with a northward upwind current along the central trough and two southward downwind coastal currents. This current field is consistent with the classic upwind current theory in a nonrotating model.

[20] The essential dynamical interplays that give arise the YSWC can be summarized in following. The curl of a uniform northerly wind stress over a trough with double shelves inputs positive PV into the western side and negative PV into the eastern side of the trough. This PV input, if not completely dissipated by friction in the trough, pushes the water moving to high PV region (toward shoreward) in

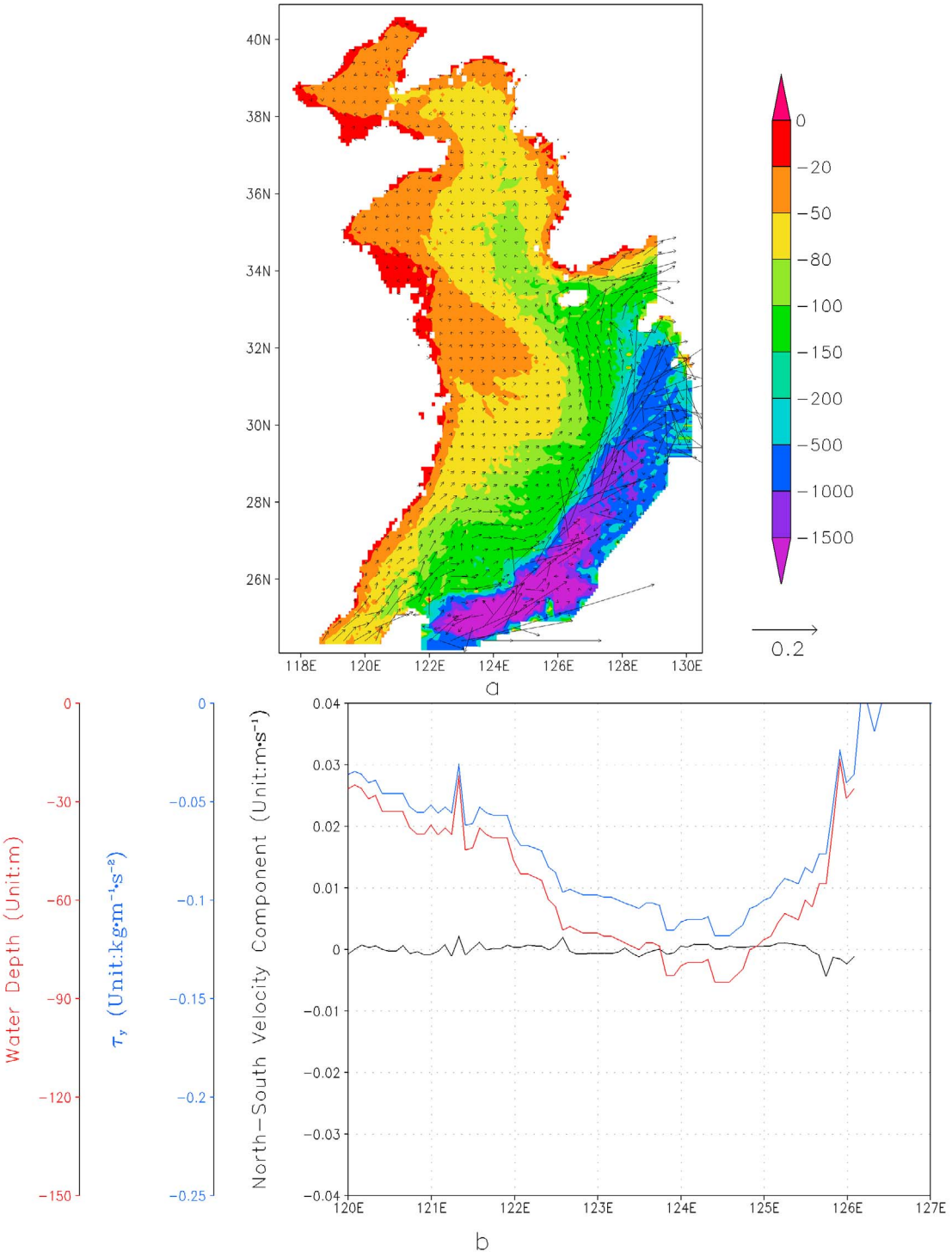

Figure 14. Results from EXP9 with a constant τ_s/H (= 0.0013). The upwind current is considerably weaker than that from EXP6 with a same friction coefficient.

the western trough and causes the asymmetric upwind current. The establishment of above equilibrium state is through the adjustment of topographic waves, which propagate along the bathymetry and are arrested by the bottom friction thereby setting up the sea level gradient which supports the steady upwind current. The discussion above is based on a one-layer dynamics. Is this model adequate for describing the essential dynamics?

[21] The premise of our conclusion is that the lowest-order dynamics for the YSWC can be represented by a barotropic model. There is no doubt that baroclinicity plays a role in any stratified ocean. Does our model overly sim-

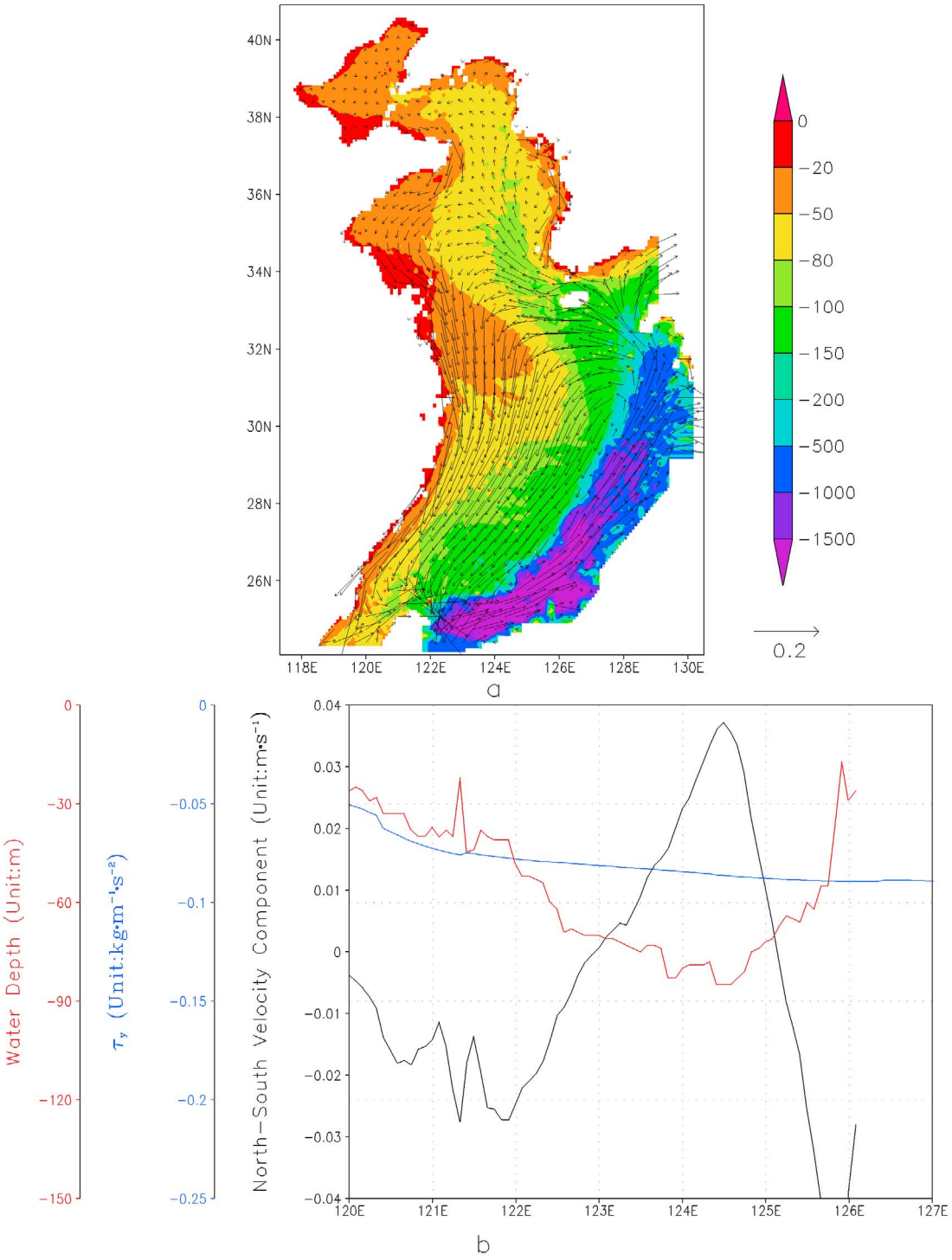

Figure 15. Results from EXP10 in a nonrotating model ($f = 0$).

plify the dynamics of YSWC? The dynamics of depth-integrated flow in a stratified ocean has been examined extensively in many previous studies [e.g., *Holland*, 1967; *Mertz and Wright*, 1992; *Hughes and de Cuevas*, 2001]. One can integrate the momentum equation from the surface to the bottom and then take the curl of the integrated flow. The linear vorticity balance with a varying bathymetry is often termed as `topographic Sverdrup relation', in a direct analog to the planetary Sverdrup balance

$$\vec{U} \cdot \nabla \frac{f}{H} = \frac{1}{\rho_0} curl\left(\frac{\vec{\tau}_s - \vec{\tau}_b - \rho_0 \nabla \Psi}{H}\right), \tag{11}$$

Table 1. Model Experiments

	Longitude (°E)	Latitude (°N)	Bathymetry	Friction Parameter λ	Coriolis Parameter f	Wind Stress Forcing τ
EXP1	8°	45°	Idealize	5×10^{-4}	35°N	0.1 N m^2
EXP2	8°	45°	Idealize	5×10^{-5}	35°N	0.1 N m^2
EXP3	8°	45°	Idealize	5×10^{-3}	35°N	0.1 N m^2
EXP4	8°	45°	Idealize	5×10^{-4}	35°N	$\tau_0/H = 0.0013$
EXP5	8°	45°	Idealize	5×10^{-4}	0	0.1 N m^2
EXP6	117°–130°	24°–41°	Realistic	5×10^{-4}	35°N	Realistic
EXP7	117°–130°	24°–41°	Realistic	5×10^{-5}	35°N	Realistic
EXP8	117°–130°	24°–41°	Realistic	5×10^{-3}	35°N	Realistic
EXP9	117°–130°	24°–41°	Realistic	5×10^{-4}	35°N	$\tau_0/H = 0.0013$
EXP10	117°–130°	24°–41°	Realistic	5×10^{-4}	0	Realistic

where U is the depth integrated velocity and $\Psi = \frac{g}{\rho_0}\int_{-H}^{0} z\rho dz$ is due to baroclinic effect (the Jacobian between Ψ and H is the Joint Effect of Baroclinicity and Relief, JEBAR). The detail derivation of (11) is given by *Mertz and Wright* [1992].

[22] Now let us first examine whether a barotropic model is adequate for our application. The depth along YST is about H = 60 m, the salinity and temperature changes between 31°N and 36°N along the YST are about 1 psu and 5°C according to observations [*Lin et al.*, 2011]. Using these numbers one obtains the magnitude of $\rho_0\nabla\Psi$ to be on the order of 10^{-2}–10^{-3} N m^{-2}. This considerably is smaller than the typical wind stress of 0.1 N m^{-2} during the winter monsoon. So the contribution from the baroclinicity to the depth-integrated transport is small. This is consistent with the velocity observations shown by *Lin et al.* [2011]. Therefore it appears to be justified that the zeroth-order dynamics be described by a barotropic PV equation

$$\vec{U}\cdot\nabla\frac{f}{H} = \frac{1}{\rho_0} curl\left(\frac{\vec{\tau}_s - \vec{\tau}_b}{H}\right). \tag{12}$$

Equation (12) is commonly called the barotropic topographic Sverdrup relation [*Holland*, 1967; *Mertz and Wright*, 1992] and is identical to the steady PV transport equation derived from our model (1). The transport includes the surface and bottom Ekman components.

[23] Why should the surface wind stress forcing depend on the water depth? Let us rederive (12) directly from barotropic equation (1). The linear vorticity equation in the steady state can be obtained by multiplying depth H in momentum equation (1) and then taking their curl

$$\beta V = gJ(\eta, H) + \frac{1}{\rho_0} curl(\vec{\tau}_s - \vec{\tau}_b), \tag{13}$$

where $gJ(\eta,H) = g(\eta_x H_y - \eta_y H_x)$ is the form drag or the bottom pressure torque. It is the vertical velocity induced by the cross-isobathic flow on the bottom. One can replace the pressure gradient term in the form drag by using the steady momentum equation from (1) and obtain (12) directly from (13). So the depth dependence of the wind stress forcing on the depth-integrated flow is actually through the form drag. The dynamics can be summarized in following: (1) with the existence of a side boundary, the Ekman transport in the Ekman layer will result in a divergence or convergence near the boundary region; (2) this divergence or convergence sets a pressure field which then forms the pressure torque due to the varied bathymetry in the bottom; and (3) the form drag, or the bottom pressure torque, will influence the flow through pressure and bathymetric variations. In a special case in which the wind stress curl is zero and the ocean is vast (no side boundary), there will be no flow beneath the Ekman layer and one can recover the Ekman transport through the vorticity equation (12).

[24] The role of the northern and southern boundaries in the model experiments needs to be discussed. In an infinitely long meridional channel with a trough in center, an upwind current cannot be formed. The existence of the northern boundary allows gyres to be formed. An alternative explanation is through the form drag. The form drag $\frac{1}{\rho}J(P,H) \approx -\frac{1}{\rho}\frac{\partial P}{\partial y}\frac{\partial H}{\partial X}$ is determined by the meridional pressure gradient, which is caused by the piling up of water in the boundaries. To maintain such pressure gradient, either the northern or the southern boundary is needed. *Hsueh* [1988] also emphasized the meridional pressure gradient from south Yellow Sea to north Yellow Sea. He concluded that the piling up of water in the south Yellow Sea is important for the formation of an upwind current in the trough region.

[25] The pressure gradient can be maintained as long as the northern boundary exists regardless whether the southern boundary is open or closed. But closing the southern boundary blocks the transient forcing from the open ocean from entering the Yellow Sea. The southern boundary also affects the spin-up processes especially when the friction is small. But when a moderate or large friction is used, the topographic waves are arrested locally by friction. In such cases, the size of the model domain becomes less important. To examine the effect of southern boundary, we conducted an additional set of experiments by using a small model domain meridionaly by 8° × 10° with a closed southern boundary. The results (not shown) are qualitatively similar to what have been shown in EXP1–EXP5.

[26] Can we apply our simple model results to a more realistic YSWC? To test our hypothesis that the interplay of wind, friction and bathymetry are the basic dynamics for the asymmetric upwind YSWC, we designed a set of experiments with realistic bathymetry, wind forcing and external circulation forcing. The model domain is from 117°E–130°E, 24°N–41°N, including the whole Bohai Sea, Yellow Sea, and East China Sea. We use the same barotropic model with a resolution of 1/16°. The bathymetry is digitized from navigation maps [*Lin et al.*, 2006]. For simplicity we treat the Ryukyu Islands as a continuous Island and there are only four straits as the open boundaries, the Taiwan Strait, the channel between Taiwan and Ryukyu Islands, the Tokara Strait and the Tsushima Strait. The open boundary conditions

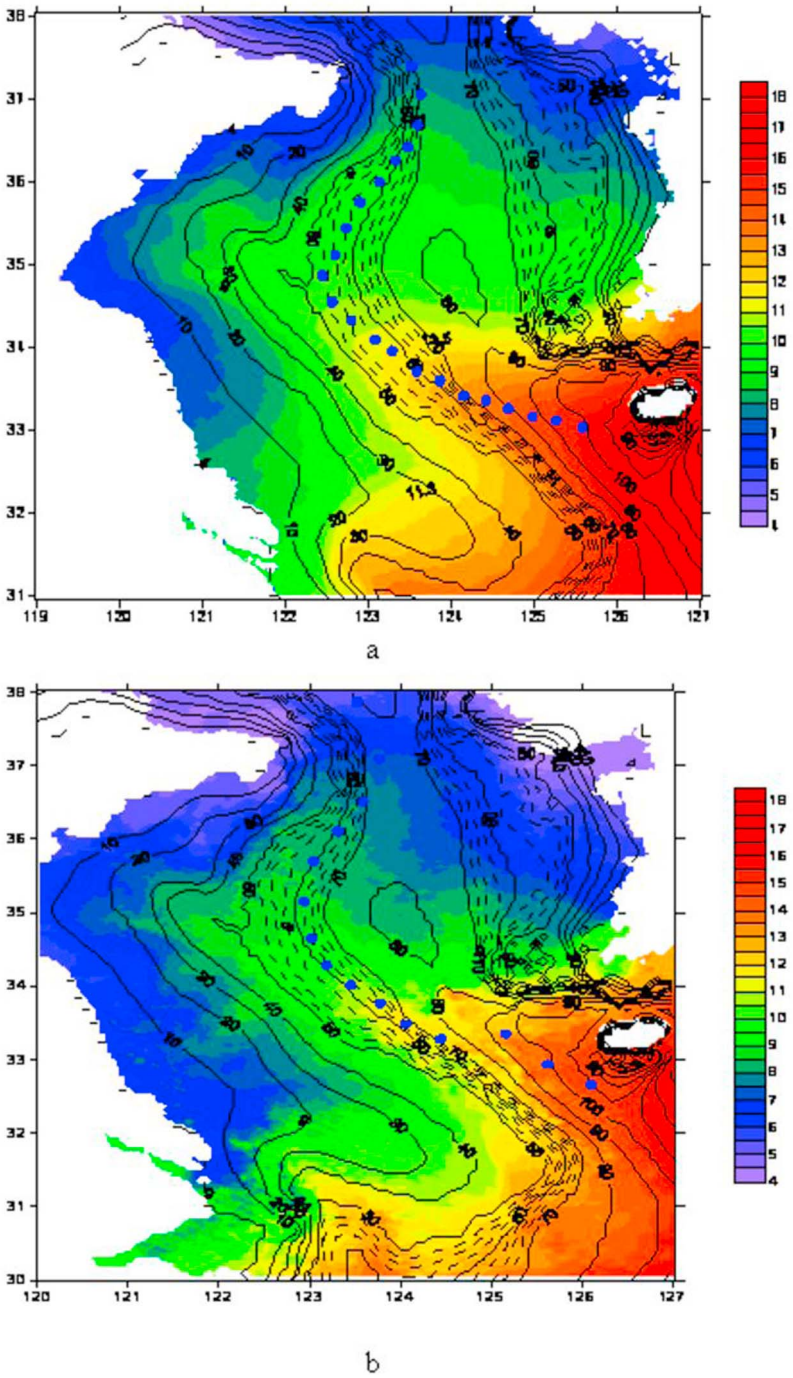

Figure 16. The mean SST in February from advanced very high resolution radiometer observations: (a) 1985–2009 and (b) 2002. The blue dots denote the axis of warm water tongue as the pathway of YSWC. The black lines are the bathymetry.

are prescribed according to results from a global model [*Liu et al.*, 2010]. The surface wind forcing is from the winter mean (DJF) climatology of QuikSCAT sea surface vector wind [*Liu*, 2002] and interpreted into the model grids. We ran a set of parallel experiments to the first set with idealized bathymetry and forcing, i.e., EXP1–EXP5. Figures 11–15 show the current fields for the EXP6–EXP10 (see Table 1 for the list). In EXP6 with a moderate friction coefficient ($\lambda = 5 \times 10^{-4}$ s^{-1} m^{-1}), the simulated YSWC is qualitatively similar to the one inferred from observations, including the westward shift of the YSWC from the YST (Figure 11). When the friction is small (EXP7, $\lambda = 5 \times 10^{-5}$), Figure 12 shows that the flow over shelves is stronger and the YSWC is shifted further westward as compared with that in EXP6. If a very large ($\lambda = 5 \times 10^{-3}$) is used (EXP8), the shelf currents are weak and the upwind flow is close to the YST (Figure 13). In EXP9, we set $\frac{\tau_0}{H}$ to be a constant (0.0013) in shelf region. The flow over the shelves is very weak and the

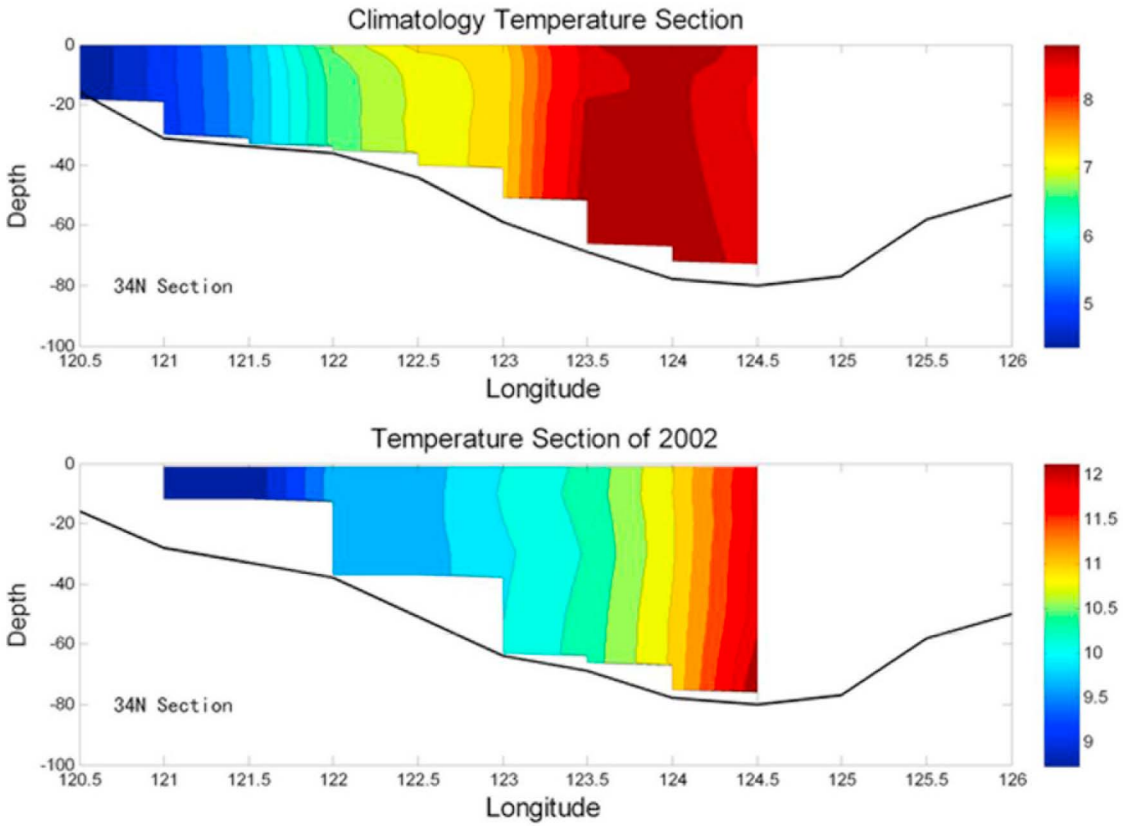

Figure 17. (top) The climatology winter temperature (1976–2007) and (bottom) the 2002 winter temperature observed in routine section 34°N (units are °C).

upwind current virtually is absent (Figure 14). In a nonrotating model with $f = 0$ (EXP10), the upwind current is along the trough as what is shown in the idealized case (Figure 15). The model result and its sensitivity to friction, wind stress and rotational effect are all similar to that with idealized bathymetry and forcing (EXP1–EXP5). They lend further support to our hypothesis that the YSWC is an upwind current arrested by friction.

[27] We have also examined our hypothesis with observations. The winter monsoon in the Yellow Sea has strong intraseasonal to interannual variability. As the dominant factor controlling the mean winter circulation pattern in the Yellow Sea, a change in the surface wind will also affect the strength and pathway of the YSWC. Such changes are evident in observations, such as the SST from satellite observations. For instance, using the maximum SST as a proxy for the axis of the YSWC, the current was aligned closer to the YST in February 2002 (Figure 16a) than the 25 year (1985–2009) February mean YSWC axis (Figure 16b). Roughly, the YSWC position in 2002 was shifted about 0.5° eastward (closer to the trough) than the 1985–2009 average position. This shift was also detectable in hydrographic data from the routine survey conducted 4 times per year along 34°N by China's State Oceanic Administration (the data source was discussed by *Lin et al.* [2011]). The mean (1976–2007) axis of the warm water along 34°N is about 123.5°E (see Figure 17, top). It shifted to the east of 124°E in 2002 winter (see Figure 17, bottom). This change in the YSWC axis may be related to a change in the surface wind in winter 2002. Figure 18 shows the curl of the depth-averaged wind stress in February for the period of 1999–2009 and in 2002. The data used here are from QuikSCAT and realistic bathymetry (the water depths digitized from navigation maps [*Lin et al.*, 2006]). Along the trough, the positive curl was considerably weaker than average in 2002. So on the western trough, the shoreward advection toward a higher f/H would be weaker than average in 2002. Consequently, the YSWC axis was closer to the trough in 2002 than what would be expected under climatological conditions.

[28] We should note that the YSWC axis is likely influenced by many factors other than local wind and bathymetry. The YSWC is connected with the Kuroshio Current, Tsushima Warm Current, and Taiwan Warm Current. Variations in these currents would inevitably influence the YSWC [*Xu et al.*, 2009]. Other factors, such as tidal forcing, directly affect the dissipation of momentum and vorticity, and thus would be expected to play a role as well in the YSWC variability. Some numerical simulations show that if the model is forced only by the external circulations, without any local wind forcing, a northward YSWC in the Yellow Sea still exists [*Jacobs et al.*, 2000; *Yang et al.*, 2006; *Moon et al.*, 2009; *Ma et al.*, 2010]. In particular, *Yang et al.* [2006] demonstrated that in a wind-driven barotropic model, like the one used in this study, but with realistic bathymetry and forcing, the Tsushima Warm

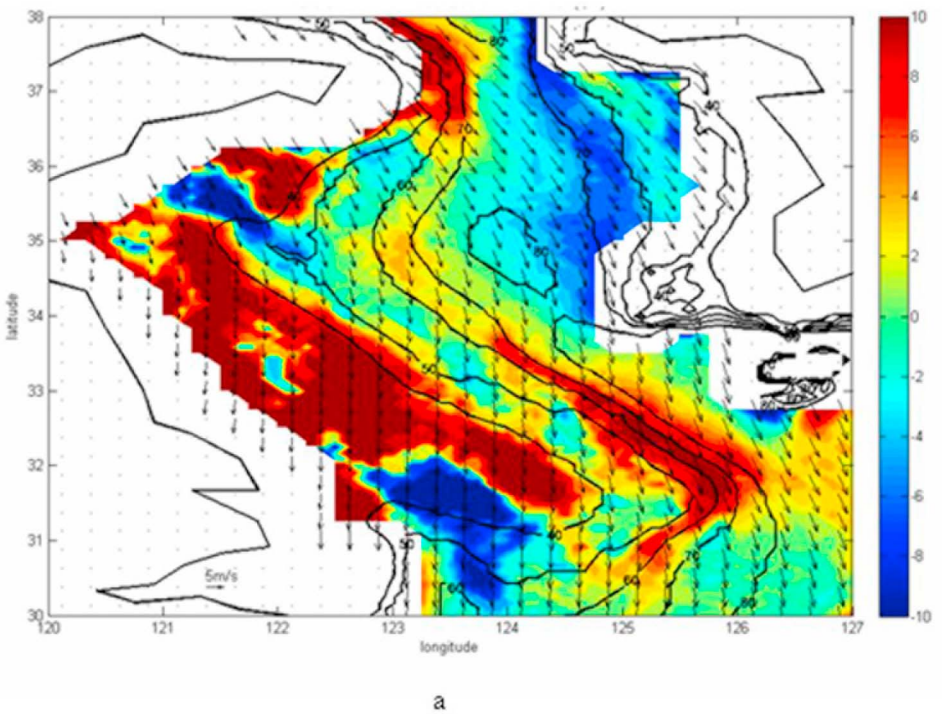

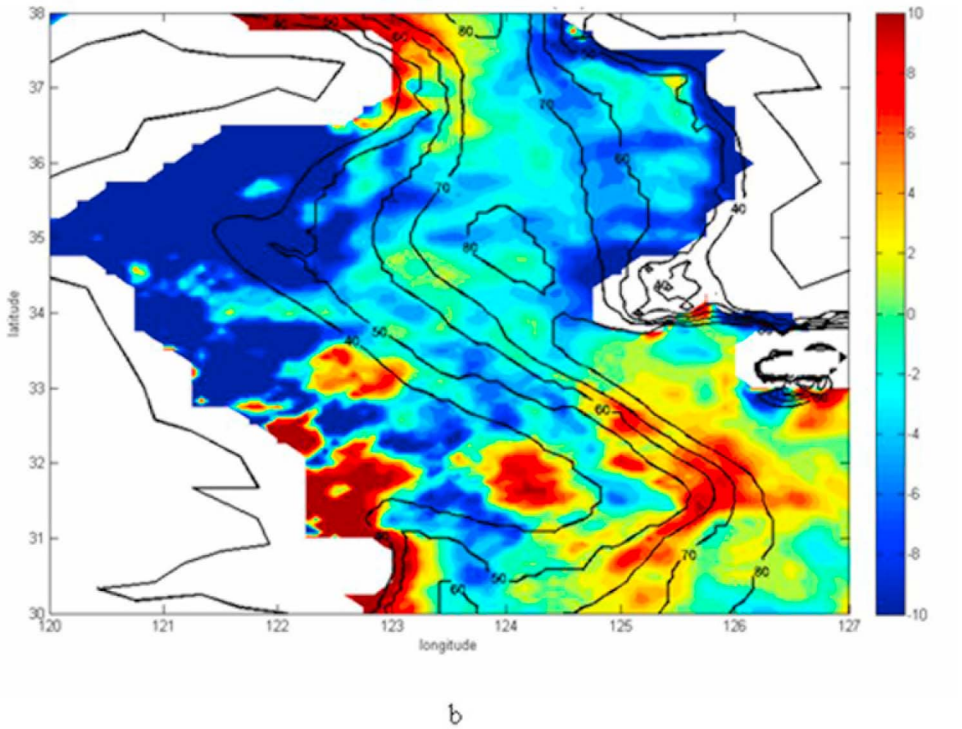

Figure 18. The PV input by wind stress (color shading, 10−7 m^{-1} s^{-1}) in February from QuikSCAT data: climatology (a) 1999–2009 and (b) 2002. The bathymetry of 40, 50, 60, 70, and 80 m are labeled by black lines.

Current (TSWC) can induce a northward flow along the Yellow Sea Trough as a source- and sink-driven flow. But the flow is very weak and usually has no obvious westward and onshore movement. In addition, it flows northward perennially like the TSWC instead of seasonally as the observed YSWC does. Our realistic experiment forced by the open boundary only also shows the similar result (figures not shown here).

[29] Tidal forcing may have a more important effect on the strength and pathway of YSWC than the external circulations. However, the tidal residual current is generally southward on the western bank of Yellow Sea trough and thus tends to reduce the northward upwind current [*Lie et al.*, 2009]. More importantly, the tidal forcing could greatly increase the bottom friction and background turbulence induced by the strong tidal currents [*Moon et al.*, 2009]. This would weaken the strength and onshore movement of YSWC.

5. Summary

[30] In this paper, we examine the zeroth-order dynamics of the YSWC by using a linear, barotropic and wind stress driven model. Our primary purpose in this study is to explore mechanisms of the YSWC and its westward shift relative to the YST. The results from 10 experiments were discussed in this study. Our analyses of PV balances indicate that the westward shift of YSWC is due to the PV input by the wind stress over YST and the position is strongly influenced by the bottom friction. Weak friction results in a runaway of the topographic waves and a steady state which is dominated by a large gyre that extends across the trough. Very large friction, on the other hand, damps the topographic waves and the final state resembles the initial flow with two symmetric gyres. A moderate friction gives an upwind current that qualitatively resembles the YSWC structure.

[31] **Acknowledgments.** X.L. has been supported by China's National Basic Research Priorities Programmer (2007CB411804 and 2005CB422303), the Ministry of Education's 111 Project (B07036), the Program for New Century Excellent Talents in University (NECT-07-0781), and the China National Science Foundation (40976004, 40921004, and 40930844). J.Y. has been supported by the U.S. National Science Foundation and the Woods Hole Oceanographic Institution's Coastal Ocean Institute. We are very grateful to Magdalena Andres (WHOI) who thoroughly reviewed the manuscript and gave many valuable comments and suggestions. Her help has considerably improved the manuscript.

References

Brink, K. H. (1998), Deep-sea forcing and exchange processes, in *The Sea*, vol. 10, *The Global Coastal Ocean: Processes and Methods*, edited by K. H. Brink and A. R. Robinson, pp. 151–167, chap. 6, John Wiley, New York.

Chapman, D. C. (1987), Application of wind-forced, long, coastal-trapped wave theory along the California coast, *J. Geophys. Res.*, *92*, 1798–1816, doi:10.1029/JC092iC02p01798.

Csanady, G. T. (1973), Wind-induced barotropic motions in long lakes, *J. Phys. Oceanogr.*, *2*, 498–508, doi:10.1175/1520-0485(1973)003%3C0429%3AWIBMIL%3E2.0.CO%3B2.

Csanady, G. T. (1978), The arrested topographic wave, *J. Phys. Oceanogr.*, *8*, 47–62, doi:10.1175/1520-0485(1978)008<0047:TATW>2.0.CO;2.

Csanady, G. T. (1982), *Circulation in the Coastal Ocean*, 279 pp., D. Reidel, New York.

Hetland, R. D., Y. Hsueh, and D. Yuan (2001), On the decay of a baroclinic jet flowing along a continental slope, *J. Geophys. Res.*, *106*, 19,797–19,807, doi:10.1029/2000JC000254.

Holland, W. R. (1967), On the wind-driven circulation in an ocean with bottom topography, *Tellus*, *19*, 582–600, doi:10.1111/j.2153-3490.1967.tb01510.x.

Hsueh, Y. (1988), Recent current observations in the eastern Yellow Sea, *J. Geophys. Res.*, *93*, 6875–6884, doi:10.1029/JC093iC06p06875.

Hsueh, Y., and I.-C. Pang (1989), Coastally trapped long waves in the Yellow Sea, *J. Phys. Oceanogr.*, *13*, 2091–2106, doi:10.1175/1520-0485(1989)019<0612:CTLWIT>2.0.CO;2.

Hsueh, Y., and D. Yuan (1997), A numerical study of the currents, heat advection and sea level fluctuations in the Yellow Sea in winter 1986, *J. Phys. Oceanogr.*, *27*, 2313–2326, doi:10.1175/1520-0485(1997)027<2313:ANSOCH>2.0.CO;2.

Hsueh, Y., R. D. Romea, and P. W. DeWitt (1986), Windertime winds and sea-level fluctuations in the northeast China Sea. Part II: Numerical model, *J. Phys. Oceanogr.*, *16*, 241–261, doi:10.1175/1520-0485(1986)016<0241:WWACSL>2.0.CO;2.

Huang, D., X. Fan, D. Xu, Y. Tong, and J. Su (2005), Westward shift of the Yellow Sea warm salty tongue, *Geophys. Res. Lett.*, *32*, L24613, doi:10.1029/2005GL024749.

Hughes, C. W., and B. A. de Cuevas (2001), Why western boundary currents in realistic oceans are inviscid: A link between form stress and bottom pressure torques, *J. Phys. Oceanogr.*, *31*, 2871–2885, doi:10.1175/1520-0485(2001)031<2871:WWBCIR>2.0.CO;2.

Isobe, A. (2008), Recent advances in ocean-circulation research on the Yellow Sea and East China Sea shelves, *J. Oceanogr.*, *64*, 569–584, doi:10.1007/s10872-008-0048-7.

Jacobs, G. A., H. B. Hur, and S. K. Riedlinger (2000), Yellow and East China seas response to winds and currents, *J. Geophys. Res.*, *105*, 21,947–21,968, doi:10.1029/2000JC900093.

Lie, H.-J. (1986), Summertime hydrographic features in the southeastern Hwanghae, *Prog. Oceanogr.*, *17*, 229–242, doi:10.1016/0079-6611(86)90046-7.

Lie, H.-J., C.-H. Choi, J.-H. Lee, S. Lee, and Y. Tang (2000), Seasonal variation of the Cheju Warm Current in the northern East China Sea, *J. Oceanogr.*, *56*, 197–211, doi:10.1023/A:1011139313988.

Lie, H.-J., C.-H. Cho, J.-H. Lee, and S. Lee (2001), Does the Yellow Sea Warm Current really exist as a persistent mean flow?, *J. Geophys. Res.*, *106*, 22,199–22,210, doi:10.1029/2000JC000629.

Lie, H.-J., C.-H. Cho, and S. Lee (2009), Tongue-shaped frontal structure and warm water intrusion in the southern Yellow Sea in winter, *J. Geophys. Res.*, *114*, C01003, doi:10.1029/2007JC004683.

Lin, X., S.-P. Xie, X. Chen, and L. Xu (2006), A well-mixed warm water column in the central Bohai Sea in summer: Effects of tidal and surface wave mixing, *J. Geophys. Res.*, *111*, C11017, doi:10.1029/2006JC003504.

Lin, X., J. Yang, J. Guo, Z. Zhang, Y. Yin, X. Song, and X. Zhang (2011), The asymmetric upwind flow, Yellow Sea Warm Current: 1. New observations on the western Yellow Sea, *J. Geophys. Res.*, *116*, C04026, doi:10.1029/2010JC006513.

Liu, N., C. Eden, H. Dietze, D. Wu, and X. Lin (2010), Model-based estimate of the heat budget in the East China Sea, *J. Geophys. Res.*, *115*, C08026, doi:10.1029/2009JC005869.

Liu, W. T. (2002), Progress in scatterometer application, *J. Oceanogr.*, *58*, 121–136, doi:10.1023/A:1015832919110.

Ma, C., D. Wu, X. P. Lin, J. Yang, and X. Ju (2010), An open-ocean forcing in the East China and Yellow seas, *J. Geophys. Res.*, *115*, C12056, doi:10.1029/2010JC006179.

Mask, A. C., J. J. O'Brien, and R. Preller (1998), Wind-driven effects on the Yellow Sea Warm Current, *J. Geophys. Res.*, *103*, 30,713–30,729, doi:10.1029/1998JC900007.

Mertz, G., and D. G. Wright (1992), Interpretation of the JEBAR term, *J. Phys. Oceanogr.*, *22*, 301–305, doi:10.1175/1520-0485(1992)022<0301:IOTJT>2.0.CO;2.

Moon, J.-H., N. Hirose, and J.-H. Yoon (2009), Comparison of wind and tidal contributions to seasonal circulation of the Yellow Sea, *J. Geophys. Res.*, *114*, C08016, doi:10.1029/2009JC005314.

Park, Y.-H. (1986), Water characteristics and movements of the Yellow Sea Warm Current in summer, *Prog. Oceanogr.*, *17*, 243–254, doi:10.1016/0079-6611(86)90047-9.

Pringle, J. M. (2002), Enhancement of wind-driven upwelling and downwelling by alongshore bathymetric variability, *J. Phys. Oceanogr.*, *32*, 3101–3112, doi:10.1175/1520-0485(2002)032<3101:EOWDUA>2.0.CO;2.

Rao, D. B., and T. S. Murthy (1970), Calculation of the steady-state wind-driven circulation in Lake Ontario, *Arch. Meteorol. Geophys. Bioklim Ser. A*, *19*, 195–210, doi:10.1007/BF02249005.

Riedlinger, S. K., and G. A. Jacobs (2000), Study of the dynamics of wind-driven transports into the Yellow Sea in winter, *J. Geophys. Res.*, *105*, 28,695–28,708, doi:10.1029/2000JC900127.

Takahashi, S., Y. Isoda, and T. Yanagi (1995), A numerical study on the formation and variation of a clockwise-circulation during winter in the Yellow Sea, *J. Oceanogr.*, *51*, 83–98, doi:10.1007/BF02235938.

Tang, Y., E. Zou, and H.-J. Lie (2001), On the origin and path of the Huanghai Warm Current during winter and early spring (in Chinese with English abstract), *Acta Oceanol. Sin.*, *23*, 1–12.

Teague, W. J., and G. A. Jacobs (2000), Current observations on the development of the Yellow Sea Warm Current, *J. Geophys. Res.*, *105*, 3401–3411, doi:10.1029/1999JC900301.

Uda, M. (1934), Hydrographical research on the normal monthly conditions in the Japan Sea, the Yellow Sea, and the Okhotsk Sea (in Japanese), *J. Imp. Fish. Exp. Stn.*, *5*, 191–236.

Uda, M. (1936), Results of simultaneous oceanographic investigations in the Japan Sea and its adjacent waters during October and November, 1933 (in Japanese), *J. Imp. Fish. Exp. Stn.*, *7*, 91–151.

Winant, C. D. (2004), Three-dimensional wind-driven flow in an elongated, rotating basin, *J. Phys. Oceanogr.*, *34*, 462–476, doi:10.1175/1520-0485(2004)034<0462:TWFIAE>2.0.CO;2.

Xie, S. P., J. Hafner, Y. Tanimoto, W. T. Liu, H. Tokinaga, and H. Xu (2002), Bathymetric effect on the winter sea surface temperature and climate of the Yellow and East China seas, *Geophys. Res. Lett.*, *29*(24), 2228, doi:10.1029/2002GL015884.

Xu, L. L., D. X. Wu, X. P. Lin, and C. Ma (2009), The study of the Yellow Sea Warm Current and its seasonal variability, *J. Hydrodynam.*, *21*, 159–165, doi:10.1016/S1001-6058(08)60133-X.

Yang, J., D. Wu, and X. Lin (2006), The Kuroshio forcing of the East Asian Marginal Seas, *Eos Trans. AGU*, *87*(36), Jt. Assem. Suppl., Abstract OS42A.

Yang, J. Y. (2007), An oceanic current against the wind: How does Taiwan Island steer warm water into the East China Sea? *J. Phys. Oceanogr.*, *37*, 2563–2569, doi:10.1175/JPO3134.1.

X. Lin, Physical Oceanography Laboratory, Ocean University of China, Qingdao 266003, China. (linxiaop@ouc.edu.cn)

J. Yang, Department of Physical Oceanography, Woods Hole Oceanographic Institution, Clark 303A, MS 21, Woods Hole, MA 02543, USA.